5230–5248 *Nucleic Acids Research, 2021, Vol. 49, No. 9* *Published online 6 May 2021*
doi: 10.1093/nar/gkab282

DNA polymerase gamma mutations that impair holoenzyme stability cause catalytic subunit depletion

Pedro Silva-Pinheiro [1,†], Carlos Pardo-Hernández [2,†], Aurelio Reyes [1], Lisa Tilokani[1], Anup Mishra[2], Raffaele Cerutti[3], Shuaifeng Li[4], Dieu-Hien Rozsivalova[5], Sebastian Valenzuela [2], Sukru A. Dogan[6], Bradley Peter[2], Patricio Fernández-Silva [7], Aleksandra Trifunovic [5], Julien Prudent[1], Michal Minczuk[1], Laurence Bindoff[8,9], Bertil Macao [2], Massimo Zeviani[3,10], Maria Falkenberg [2,*,†] and Carlo Viscomi[11,*,†]

[1]MRC/University of Cambridge Mitochondrial Biology Unit, Hills Road, CB2 0XY Cambridge, UK, [2]Department of Medical Biochemistry and Cell Biology, University of Gothenburg, Medicinaregatan 9A P.O. Box 440, SE405 30 Gothenburg, Sweden, [3]Department of Neurosciences, University of Padova, via Giustiniani, 2-35128 Padova, Italy, [4]Center for Cancer Biology, Life Science of Institution, Zhejiang University, Hangzhou 310058, China, [5]Cologne Excellence Cluster on Cellular Stress Responses in Aging-Associated Diseases (CECAD) and Center for Molecular Medicine (CMMC), University of Cologne, Joseph-Stelzmann-Strasse 26, 50931 Cologne, Germany, [6]Department of Molecular Biology and Genetics, Center for Life Sciences and Technologies, Bogazici University, 34342 Istanbul, Turkey, [7]Biochemistry and Molecular and Cell Biology Department, University of Zaragoza, C/ Pedro Cerbuna s/n 50.009-Zaragoza, and Biocomputation and Complex Systems Physics Institute (BIFI), C/ Mariano Esquillor, 50.018-Zaragoza, Spain, [8]Department of Clinical Medicine, University of Bergen, 5007 Bergen, Norway, [9]Neuro-SysMed, Department of Neurology, Haukeland University Hospital, Jonas Lies vei 65, 5021 Bergen, Norway, [10]Venetian Institute of Molecular Medicine, via Orus 2-35128 Padova, Italy and [11]Department of Biomedical Sciences, University of Padova, via Ugo Bassi 58/B-35131 Padova, Italy

Received December 15, 2020; Revised March 29, 2021; Editorial Decision April 01, 2021; Accepted April 08, 2021

ABSTRACT

Mutations in *POLG*, encoding POLγA, the catalytic subunit of the mitochondrial DNA polymerase, cause a spectrum of disorders characterized by mtDNA instability. However, the molecular pathogenesis of *POLG*-related diseases is poorly understood and efficient treatments are missing. Here, we generate the *Polg*$^{A449T/A449T}$ mouse model, which reproduces the A467T change, the most common human recessive mutation of *POLG*. We show that the mouse A449T mutation impairs DNA binding and mtDNA synthesis activities of POLγ, leading to a stalling phenotype. Most importantly, the A449T mutation also strongly impairs interactions with POLγB, the accessory subunit of the POLγ holoenzyme. This allows the free POLγA to become a substrate for LONP1 protease degradation, leading to dramatically reduced levels of POLγA in A449T mouse tissues. Therefore, in addition to its role as a processivity factor, POLγB acts to stabilize POLγA and to prevent LONP1-dependent degradation. Notably, we validated this mechanism for other disease-associated mutations affecting the interaction between the two POLγ subunits. We suggest that targeting POLγA turnover can be exploited as a target for the development of future therapies.

*To whom correspondence should be addressed. Tel: +39 49 8276458; Email: carlo.viscomi@unipd.it
Correspondence may also be addressed to Maria Falkenberg. Tel: +46 31 786444; Email: maria.falkenberg@medkem.gu.se
†The authors wish it to be known that, in their opinion, the first two and last two authors should be regarded as Joint First and Last Authors, respectively.

GRAPHICAL ABSTRACT

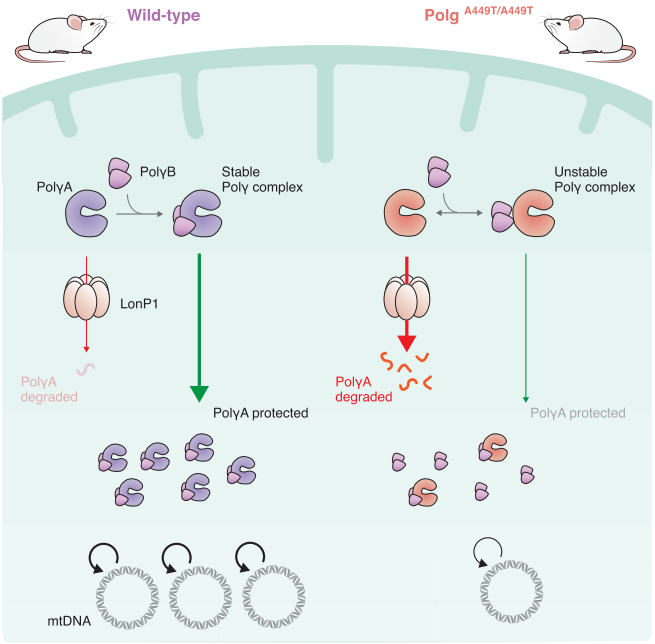

INTRODUCTION

DNA polymerase γ (POLγ) is the main protein responsible for mitochondrial DNA (mtDNA) replication and mutations in its gene (*POLG*) are the most frequent cause of mitochondrial disease related to a single nuclear gene. POLγ consists of a heterotrimer with one catalytic POLγA subunit and two POLγB accessory subunits (1). The *POLG* gene codes for the 140 kDa POLγA subunit that harbors DNA polymerase, 3′-5′ exonuclease and 5′-deoxyribose phosphate lyase activities (2,3), whereas *POLG2* encodes the 55 kDa POLγB, which stabilizes the interactions with template-DNA, thereby increasing processivity (4). POLγ is the only DNA polymerase required for mtDNA replication in mammalian mitochondria and, at the replication fork, it works in concert with the TWINKLE DNA helicase (5). The mitochondrial single-stranded DNA-binding protein (mtSSB) stimulates mtDNA synthesis by increasing the helicase activity of TWINKLE and the DNA synthesis activity of POLγ (6).

The A467T is the most frequent POLγA mutation in Scandinavian and Northern European countries, together with another change, the W748S change, which seems to be part of the Finnish disease heritage (7–10). The intermediate region, where the two deleterious mutations are located, is defined as the 'linker' region between the proofreading and the polymerase domain and seems to play a role in the binding to the accessory subunit POLγB. The mechanistic explanation of how these two mutations affect the activity of this important enzyme and lead to disease is not fully understood, but *in vitro*, the A467T mutation reduces POLγA affinity for the POLγB accessory subunit and impairs the catalytic activity of POLγ (11). In addition to the A467T and W748S, over 300 mutations have been described in *POLG* (Human DNA Polymerase Gamma Mutation Database: https://tools.niehs.nih.gov/polg/). However, four mutations alone (A467T, W748S, G848S and the T251I–P587L allelic pair) account for ∼50% of all mutations identified in patients with *POLG*-related diseases, with ∼75% of patients carrying at least one of these mutant alleles (12). *POLG* mutations may lead to mtDNA instability, causing either multiple deletions or depletion (13). However, there is no obvious genotype–phenotype correlation, the same mutation can often lead to mtDNA deletions, mtDNA depletion or both. A prototypical example is the homozygous mutation A467T mutation, which has been associated with a range of phenotypes, from severe conditions such as Alpers-Huttenlocher syndrome to milder ones such as myoclonic epilepsy myopathy sensory ataxia, comprising spinocerebellar ataxia with epilepsy, frequently associated with sensory ataxia neuropathy with dysarthria and ophthalmoplegia (14).

In addition, the age of onset and the progression of POLG-related disease in patients with the same *POLG* mutations is astonishingly variable and can span several decades. For instance, the onset of disease spans >70 years in compound heterozygous patients carrying the T251I–P587L mutations on one allele (15) and the G848S mutation on the other, and it spans at least four decades of life in homozygous A467T patients (16,17).

Maintaining mitochondrial protein homeostasis (proteostasis) is essential for most mitochondrial processes, including those involved in mtDNA maintenance. Mitochondrial proteostasis is ensured by proteases, which are involved in the regulation of the protein steady-state levels and degrade misfolded and/or unincorporated peptides. A particularly relevant role is carried out by LONP1, a AAA^+ protease of the mitochondrial matrix (18). LONP1 has three functional domains: a substrate recognition N-terminal domain, an adenosine triphosphate (ATP)-binding and hydrolyzing AAA^+ ATPase domain and a C-terminal protease domain. The LONP1 protein forms a hexameric cylindrical structure which recognizes its substrates and carries out protein unfolding and proteolysis in an ATP-dependent manner. In addition, LONP1 influences mtDNA levels by degrading the mitochondrial transcriptional factor A (TFAM) (19–21), a key factor in regulation of mitochondrial transcription initiation and packaging of mtDNA into nucleoprotein structures (nucleoids) (22). Notably, LONP1 mutations have been associated with mitochondrial disease (23).

We here establish a disease model, which reproduces the human A467T change in the mouse ($Polg^{A449T/A449T}$). *In vitro,* the mouse mutation, A449T, impacts polymerase activity in a way similar to what has been previously described for human A467T (11). Interestingly, analysis of $Polg^{A449T/A449T}$ mouse tissues reveals a dramatic depletion of mutant POLγA. We find that this depletion is explained by weakened interactions with POLγB. When POLγA is not bound to POLγB, it is susceptible to degradation by LONP1. Our results demonstrate a protective role for POLγB and reveal a novel pathogenic mechanism for *POLG*-related diseases, which in turn may open new avenues for the development of future therapies.

MATERIALS AND METHODS

Generation of *Polg*$^{A449T/A449T}$ mice

Polg$^{A449T/A449T}$ mice were generated by a double-nickase CRISPR/Cas9 D10A-mediated gene editing of mouse *Polg* gene in exon 7 (c.1345G>A/p.A449T). For a detailed representation see Supplementary Figure S1A. The selected sgRNAs (Table 1) were cloned into plasmid pSpCas9(BB)-PX330 (Addgene #42230), using the BbsI site. The resulting constructs were used as a template to amplify by polymerase chain reaction (PCR) the gRNA (spacer + scaffold) preceded by a T3 promoter to allow subsequent *in vitro* transcription. The *in vitro* transcription was carried using the MEGAscript T3 Transcription Kit (Life Technologies). The same kit was used to produce Cas9 D10A mRNA using as template the plasmid pCAG-T3-hCasD10A-pA (Addgene #51638). The 140 bp ssDNA homology direct repair (HDR) donor (Table 1) was acquired from IDT. Cas9 D10A mRNA, gRNAs and HDR donor were microinjected into fertilized FVB/NJ one-cell embryos (Core Facility for Conditional Mutagenesis, Milan). Genotyping of *Polg*$^{A449T/A449T}$ mice was performed by PCR (primers Polg_A449T_Fw + Polg_A449T_Rv, Table 1), followed by a restriction digestion with PvuII. Wild-type (WT) allele produces a fragment of 769 bp, which is cleaved in the A449T allele producing two fragments of 490 + 279 bp (Supplementary Figure S1B). The PCR is carried using GoTaq DNA polymerase (Promega, UK) and the following PCR conditions: 95 °C for 30 s, 63.7 °C for 30 s and 72 °C for 1 min, 35 cycles.

Animal work

All animal experiments were carried out in accordance with the UK Animals (Scientific Procedures) Act 1986 (PPL: P6C20975A) and EU Directive 2010/63/EU. The mice were kept on FVB/NJ background, and WT littermates were used as controls. The animals were maintained in a temperature- and humidity-controlled animal care facility with a 12-h light/12-h dark cycle and free access to water and food, and they were monitored weekly to examine body condition, weight and general health. The mice were sacrificed by cervical dislocation at 3, 12 and 24 months of age for subsequent analysis.

Lonp1 gene targeting (*Lonp1*$^{+/tm1a(EUCOMM)Hmgu/Ieg}$, project number HEPD0936_3_B11) was carried out as part of the The European Conditional Mouse Mutagenesis Program (EUCOMM), on the C57BL/6NTac genetic background. We generated the heart and skeletal muscle (SKM)-specific *Lonp1* knockout mice by mating *Lonp1*$^{fl/fl}$ animals with transgenic mice expressing cre recombinase under the control of muscle creatine kinase promoter (*Ckmm-cre*) (19), after removal of a gene-trap DNA cassette. Experiments were performed on 12-week-old mice. The genotyping primers used are on Table 1 (Lonp1_KO_Fw + Lonp1_KO_Rv).

All experiments on *Lonp1*$^{fl/fl}$*; Ckmm-Cre* animals were approved and permitted by the Animal Ethics Committee of North-Rhein Westphalia (Landesamt für Natur, Umwelt und Verbraucherschutz Nordrhein-Westfalen; LANUV) following the German and European Union regulations.

Treadmill

A standard treadmill apparatus (Panlab) was used to measure motor endurance according to the number of falls in the motivational air puff during a gradually accelerating program with speed initially at 6.5 m/min and increasing by 0.5 m/min every 3 min. The test was terminated by exhaustion, defined as >10 air puffs activations/min.

Comprehensive laboratory animal monitoring system (CLAMS)

Mice were individually placed in the CLAMS™ system of metabolic cages and monitored over a 48-h period. Data were collected every 10 min. The parameters analyzed were: ambulatory and rear movements, VO_2 (volume of oxygen consumed, ml/kg/h), VCO_2 (volume of carbon dioxide produced, ml/kg/h), RER (respiratory exchange ratio) and heat (kcal/h).

Pharmacological treatments

In VPA-treated mice, VPA (Sigma) was administrated by daily oral gavage (300 mg/kg in water) or added to a standard diet at 1.5% (1.5 g VPA/1 kg food) and administered for 60 days, starting at 8 weeks of age.

In CCl_4 experiments, mice received a single IP injection of CCl_4 (1 ml/kg body weight diluted 1/10 in olive oil (Sigma). Mice were sacrificed after 2 or 4 days. For histology analysis of necrotic areas (see below), Hematoxylin and Eosin (H&E) staining was performed in livers samples. The quantification of necrotic areas was done with ImageJ by dividing the necrotic areas around the central veins by total area of the section. Five different regions of the slide were analyzed and average value obtained.

DNA and RNA extraction

Genomic DNA was extracted by resuspending samples in lysis buffer (0.5% sodium dodecyl sulfate (SDS); 0.1 M NaCl; 50 mM Tris–HCl, pH = 8; 2.5 mM EDTA). Samples were incubated overnight at 55°C after adding Proteinase K (final concentration: 20 ng/μL). Next, samples were purified with 1 volume chloroform + 0.6 M potassium acetate and the supernatant was ethanol precipitated. Final DNA was eluted in water.

Total RNA was extracted from the indicated tissues using the TRIzol Reagent (Thermofisher) following the manufacture protocol.

Real-time quantitative PCR

For mtDNA relative quantification, SYBR Green real-time qPCR was performed using primers specific to a mouse mtDNA region in the COI gene. Primers specific to RNaseP, a single copy gene taken as a nuclear gene reference. All primers are listed in Table 1. Approximately 25 ng of DNA was used per reaction.

For the quantification of mRNA levels, cDNA was retrotranscribed from total RNA extracted using the Omniscript RT kit (Qiagen). For mitochondrial transcripts *CoI* and *Nd4*, specific primers (Table 1) were used as described above

Table 1. Oligonucleotides list

Name	Sequence (5′- 3′)	Use
sgRNA-Fw	GATGCCTGTCAGTTGCTCTC	$Polg^{A449T/KO}$ generation
sgRNA-Rv	GCGACTTCTTCATCTCCCGC	
140 bp ssDNA HDR donor	AGGCACAGAACACATATGAGGAGCTACAGCGGGAGA	
	TGAAGAAGTCGCTGATGGATCTGACTAATGATGCCTGT	
	CAGCTGCTCTCAGGAGAGAGGTAGTCAGGTTCTGGG	
	CAGGCTGGGTCAATGCAGGGTACAGGCAGG	
Polg_A449T_Fw	GTTGTCCCTGTCTTCCTCCA	Genotyping
Polg_A449T_Rv	AAGCTTCCCACCTTCCTGAT	
Polg_KO_Fw1	CTTCGTCGATCGACCTCGAATAAC	
Polg_KO_Fw2	GGATGGGCAGGAACAGTTAG	
Polg_KO_Rv	CTGCCATTCACCTTACCC	
Lonp1_KO_Fw	AGGTGACTGTGGAGAGATTCC	
Lonp1_KO_Rv	CTTCACTAGTGTCACAGACCT	
qPCR_mCoI_Fw	TGCTAGCCGCAGGCATTACT	qPCR and rt-qPCR
qPCR_mCoI_Rv	CGGGATCAAAGAAAGTTGTGTTT	
qPCR_RnaseP_Fw	GCCTACACTGGAGTCGTGCTACT	
qPCR_RnaseP_Rv	CTGACCACACGAGCTGGTAGAA	
qPCR_mNd4_Fw	TCGCCTACTCCTCAGTTAGCCA	
qPCR_mNd4_Rv	GATGTGAGGCCATGTGCGATT	
qPCR_Gapdh_Fw	CACCATCTTCCAGGAGCGAG	
qPCR_Gapdh_Rv	CCTTCTCCATGGTGGTGAAGAC	
LongR_mtDNA_Fw	GAGGTGATGTTTTTGGTAAACAGGCGGGGT	Long-range PCR
LongR_mtDNA_Fw	GGTTCGTTTGTTCAACGATTAAAGTCCTACGTG	
7S_probe_Fw	ATCAATGGTTCAGGTCATAAAATAATCATCAAC	Southern Blot
7S_probe_Rv	GCCTTAGGTGATTGGGTTTTGC	

with SYBR Green chemistry. Expression was calculated using the ΔΔCt analysis using *Gapdh* as reference.

Specific Gene Expression TaqMan assays (Invitrogen) were used for *Polg* and *Polg2*. Expression was calculated using the ΔΔCt analysis using *B2m* as reference.

Long-range PCR

MtDNA was amplified from 50 ng of total DNA with the primers (LongR_mtDNA_Fw and LongR_mtDNA_Rv, Table 1) using PrimeSTAR GXL DNA polymerase (TAKARA, Japan) and following PCR conditions: 98°C for 10 s, 68°C for 13 min, 35 cycles.

Cell cultures

$Polg^{A449T/A449T}$ and control mouse embryonic fibroblasts (MEFs) were prepared from individual E12.5 embryos and were cultured in complete Dulbecco's Modified Eagle Medium (DMEM) (4.5 g/L glucose 2 mM glutamine, 110 mg/ml sodium pyruvate), supplemented with 10% fetal bovine serum (FBS) and 5% penicillin/streptomycin. MEFs were seeded in six-well plates at 20% confluence. Cells were incubated with or without 100 ng/mL EtBr for 5 days and DNA samples were collected every 24h. At day 5, new medium without EtBr was added and cells were allowed to recover for an additional 8 days. Again, DNA samples were collected every 24h. MtDNA quantification was performed as described above.

HeLa cells were grown at 37 °C, 5% CO_2 in DMEM (4.5 g/L glucose, 2 mM glutamine, 110 mg/ml sodium pyruvate) supplemented with 10% FBS and 5% penicillin/streptomycin. For siRNA transfections, 0.3×10^6 HeLa cells were reverse transfected with 5 nM of siRNA using Lipofectamine RNAiMAX. siRNAs used in the study are: (i) *LONP1* (5′-GGUGCUGUUCAUCUGCACGtt-3′), (ii) *POLG2* (5′-CGGUGCCUUGGAACACUAUtt-3′), (iii) *POLG* (5′- CCCAUUGGACAUCCAGAUGtt-3′). After 3 days, cells were harvested, washed with PBS and used for western blotting as described below.

Immunofluorescence analysis and confocal imaging

Immunofluorescence was performed as previously described (24). Briefly, cells seeded in 24-well plate were fixed in 5% paraformaldehyde (PFA) in PBS at 37 °C for 15 min and incubated with 50 mM ammonium chloride in PBS for 10 min at room temperature (RT). After three washes in PBS, cells were permeabilized using 0.1% Triton X- 100 in PBS for 10 min, washed three times with PBS, and then blocked in 10% FBS in PBS for 20 min at RT. Cells were then incubated with indicated primary antibodies for 2 h in 5% FBS/PBS, washed in 5% FBS in PBS and incubated with secondary Alexa Fluor conjugated antibodies in 5% FBS/PBS for 1 h at RT. We used the following antibodies: TOM20 (1:1000) was from Abcam (ab232589), DNA (1:1500) was from Millipore (CBL186), Goat Anti-rabbit Alexa Fluor 594 (1:1000) was from Invitrogen (A-11012), Donkey anti-mouse Alexa Fluor 488 (1:1000) was from Invitrogen (A-21202). EdU incorporation was detected using Invitrogen Click-iT EdU AlexaFluor 647 (Invitrogen, C10340) labeling kit according to manufacturer's instructions. Coverslips were mounted onto sides using Dako fluorescence mounting medium (Dako). Images were then acquired as 7 stacks of 0.2 μm each, using a 100× objective lense (NA1.4) on a Nikon Eclipse TiE inverted microscope using an Andor Dragonfly 500 confocal spinning disk system, equipped with a Zyla 4.2 PLUS sCMOS camera, exciting with 488 nm, 594 nm or 633 nm lasers, and coupled with Fusion software (Andor). For quantification of EdU or mtDNA number, max projection images were

processed once with the 'smooth' function in Fiji and nucleus was removed. Images were then manually thresholded, 'smoothed' and number of particles were obtained using the 'Analyze particles' plugin in Fiji with a minimum area of 0.1 μm^2. The representative images in Figure 3 were processed once with the 'smooth' function in Fiji.

Biochemical analysis of MRC complexes

Liver and muscle samples stored in liquid nitrogen were homogenized in 10 mM of potassium phosphate buffer (pH = 7.4), and the spectrophotometric activity of respiratory chain complexes I, II, III and IV, as well as citrate synthase, was measured as described (25).

BNGE and in-gel activity

For blue native gel electrophoresis (BNGE) analysis, SKM and liver mitochondria were isolated as previously described (26). Samples were resuspended in 1.5 M aminocaproic acid, 50 mM Bis-Tris/HCl (pH 7) and 4 mg of dodecyl maltoside/mg of protein, and incubated for 5 min on ice before centrifuging at 20,000 × g at 4 °C. 5% Coomassie G250 was added to the supernatant. 100 μg was separated by 4%–12% gradient BNGE and further subjected to a Complex I in-gel activity (IGA), as previously described (27). To allow for cI activity to appear, gels were incubated between 1.5 and 24 h in cI-IGA reaction buffer.

Histological analysis

Mouse tissues for Hematoxylin and Eosin (H&E) analysis, were fixed in 10% neutral buffered formalin (NBF) for a few days at room temperature and then included in paraffin wax. Sections of 4 μm were used for analysis. H&E staining was performed by the standard methods.

For COX/SDH histochemical analysis, SKM (gastrocnemius) samples were frozen in isopentane pre-cooled in liquid nitrogen. Sections of 8 μm were stained for COX and SDH activity as described (28).

Southern blot

Three micrograms of total DNA isolated from each tissue were restricted using the restriction enzyme *BlpI* according to manufacturer's instructions (New England Biolabs). Products were separated on 0.8% agarose gels (Invitrogen Ultrapure) and dry-blotted overnight onto nylon membrane (GE Magnaprobe). Membranes were hybridized with radiolabeled probes overnight at 65 °C in 0.25 M phosphate buffer (pH 7.6) and 7% SDS, then washed for 3 × 20 min in 1 × SSC and 0.1% SDS and imaged using a phosphorimager (GE Healthcare) and scanned using an Amersham Typhoon 5 scanner. For primer sequences used for producing probes, see Table 1.

In organello replication

Labeling of mtDNA in isolated organelles was performed as previously described (29).

Briefly, isolated liver was minced and homogenized in 4 ml/g of tissue in Sucrose-Tris-EDTA (STE)-buffer [320 mM sucrose, 10 mM Tris–HCl (pH 7.4), 1 mM ethylenediaminetetraacetic acid (EDTA) and 1 mg/ml essentially fatty acid–free bovine serum albumin (BSA)] using a manual tight-fitting teflon pestle. Resulting mitochondria were washed once in STE-buffer, pelleted and equilibrated in incubation buffer [10 mM Tris–HCl (pH 8.0), sucrose and glucose 20 mM each, 65 mM D-sorbitol, 100 mM KCl, 10 mM K_2HPO_4, 50 μM EDTA, 1 mg/ml BSA, 1 mM ADP, $MgCl_2$, glutamate and malate 5 mM each]. In organello labeling was performed for 5; 15; 30; 60 and 90 min at 37 °C with rotation, using 1 mg/ml mitochondria in incubation buffer supplemented with dCTP, dGTP and dTTP (50 μM each) and [α-^{32}P]-dATP (Hartmann, 3000 Ci/mmol) at 6.6 nM. At the end, DNA was extracted by solubilizing mitochondria with 1% sodium N-lauroylsarcosinate, followed by 100 μg/ml Proteinase K on ice for 30 min and phenol–chloroform extraction. Gel electrophoresis, Southern blotting and hybridization were carried as described above.

2D-AGE

For 2D gels, DNA was extracted from fresh liver-isolated mitochondria purified by sucrose gradient followed by phenol–chloroform extraction. Five micrograms of the resulting mtDNA were restricted digested with BclI according to manufacturer's instructions (New England Biolabs). For first dimension, products were separated on 0.4% agarose gels (Invitrogen Ultrapure) without ethidium bromide. Then each lane was excised and rotated 90° anticlockwise for second dimension electrophoresis by casting around the gel slices 1% agarose with 500 ng/ml ethidium bromide. After electrophoresis, Southern blotting and hybridization were carried as described above.

Western blot and antibodies

Mouse tissues were homogenized in RIPA buffer [150 mM sodium chloride, 1.0% NP-40, 0.5% sodium deoxycholate, 0.1% SDS, 50 mM Tris, pH 8.0] in the presence of protease inhibitors (cOmplete™ Protease Inhibitor Cocktail, Sigma). Protein concentration was determined by the Lowry method. Aliquots, 30 μg each, were run through a 12% SDS-polyacrylamide gel electrophoresis (SDS-PAGE) and electroblotted onto a polyvinylidene fluoride (PVDF) membrane, which was then immunodecorated with different primary antibodies: anti-POLγA (1:500) was from Santa Cruz Biotechnology (sc-5931), anti-POLγB (1:1000) was from LSBio (LS-C334882), anti-GAPDH (1:3000) was from Abcam (ab53098), anti-LONP1 (1:1000) was from Proteintech (15440–1-AP), anti-HSC70 (1:1000) was from Santa Cruz Biotechnology (sc-7298). Secondary antibodies were from Promega (catalog nos. W4011 [rabbit], W4021 [mouse] and V8051 [goat]). HeLa cells were lysed in lysis buffer (0.125 M Tris–HCl, pH. 6.8., 4% SDS and 500 mM NaCl). Whole cell lysates were quantified and 50 μg were resolved in 4–20% SDS-PAGE and transferred onto nitrocellulose membranes (GE healthcare). The membranes were then incubated with the primary antibodies: anti-POLγA (1:1000) was from Abcam (ab128899), anti-POLγB (1:500) was home-made polyclonal from Agrisera, anti-LONP1 (1:1000) was from Abcam (cat ab103809) and anti-β-actin (1:10000) was from Abcam (ab6276).

Quantification of POLγB and POLγA in mouse tissues was performed with enriched mitochondria fractions. Mouse tissues were homogenized in buffer A [320 mM sucrose, 1 mM EDTA, 10 mM Tris–HCl, pH 7.4] followed by a centrifugation at 800 × *g* for 5 min. The supernantant was further centrifuged at 12 000 × *g* for 2 min and the resulting mitochondria-enriched pellet was lysed with RIPA buffer and treated as described above. Each well was loaded with 10 μg of mitochondria-enriched protein extracts. Absolute quantification was performed using a standard curve with known protein concentrations of purified recombinant POLγA and POLγB. Ratio between POLγB (calculated as a dimer) and POLγA was calculated by dividing POLγB amount by 2 to obtain the amount of POLγB dimer. The final value was obtained by dividing the amount of POLγB dimer by the amount of POLγA. Ratio of (POLγB dimer)/ POLγA for HeLa cells was obtained with a similar method by using whole cell lysates as described above. During the course of our experiments, we noted that native POLγB migrates with an apparent molecular weight slightly higher than expected from predictions. The results were the same with two different antibodies (LS-Bio LS-C334882 and Agrisera) and the specific recognition of the protein was verified by siRNA-dependent depletion of POLγB in HeLa cells.

Production of LONP1, TFAM, POLγA and POLγB, expression and purification

LONP1 (WT and LONP1^{S855A}) gene lacking the mitochondrial targeting sequence (aa 1–67) was cloned into a pNic28-BSA4 vector with a cleavable 6×HisTag in the N-terminus. Rosetta™(DE3) pLysS competent cells (Novagen) were transformed with the plasmid and grown in Terrific Broth media with 50 mg/l Ampicillin and 34 mg/l Chloramphenicol at 37°C until OD_{600} = 3. Protein expression was induced with 1 mM IPTG at 16 °C for 4 h.

Cells were harvested by centrifugation, frozen in liquid nitrogen, thawed and lysed at 4 °C in lysis buffer (25 mM Tris-HCl pH 8.0, 0.8 M NaCl and 10 mM β-mercaptoethanol). The suspension was homogenized using an Ultra-Turrax T3 homogenizer (IKA) and centrifuged at 20 000 × *g* for 45 min in a JA-25.50 rotor (Beckman Coulter). The supernatant was loaded onto His-Select Nickel Affinity Gel (Sigma-Aldrich) equilibrated with buffer A (25 mM Tris–HCl, pH 8.0, 0.4 M NaCl, 10% glycerol and 10 mM β-mercaptoethanol). The protein was eluted with buffer A containing 250 mM imidazole. Removal of the 6×HisTag was achieved by overnight dialysis in presence of ≈0.5 mg TEV in buffer A. An additional Nickel purification step was performed to get rid of uncut His tagged protein and TEV. The protein was subsequently purified over a 5-ml HiTrap Heparin HP column (GE Healthcare) and a 1-ml HiTrap Q HP column (GE Healthcare), both equilibrated in buffer B (25 mM Tris–HCl pH 8.0, 10% glycerol and 1 mM DTT) containing 0.2 M NaCl, followed by elution driven by a linear gradient (50 and 10 ml, respectively) of buffer B containing 1.2 M NaCl (0.2–1.2 M NaCl). Protein purity was checked on a precast 4–20% gradient SDS-PAGE gel (BioRad, 567–8094) and pure fractions were aliquoted and stored at −80 °C. TFAM was expressed in bacteria and purified as previously described (20).

Human and mouse POLγA versions (lacking the mitochondrial targeting sequence aa 1–25) and human and mouse POLγB (lacking the mitochondrial targeting sequence aa 1–24 and aa 1–16, respectively) were expressed in Sf9 cells and purified as described previously (30), with the following modifications. For POLγA, an additional step of purification with 1 ml HiTrap SP HP column was added after the HiTrap Q HP column purification. The column was equilibrated with buffer B containing 0.1 M NaCl and eluted with a linear gradient (10 ml) of buffer B containing 1.2 M NaCl (0.1–1.2 M NaCl). For POLγB, an additional step of purification with a 1-ml HiTrap Talon column (GE Healthcare) was used in between HiTrap Heparin HP (GE Healthcare) and HiTrap SP HP (GE Healthcare). This column was equilibrated with buffer C (25 mM Hepes pH 6.8, 10% glycerol, 0.4 M NaCl, 1 mM β-mercaptoethanol) containing 5 mM imidazole and elution driven by a linear gradient (10 ml) of buffer C containing 150 mM imidazole (5–150 mM imidazole).

For the generation of mutant versions of POLγA, QuikChange Lightning Site-Directed Mutagenesis Kit (Agilent, #210519) was used according to manufacturer's indications.

Electrophoresis mobility shift assay (EMSA)

DNA binding affinity of POLγA and POLγA-B2 to a primer-template was assayed using a 36-nucleotide (nt) oligonucleotide [5′-TTTTTTTTTTATCCGGGC TCCTCTAGACTCGACCGC-3′] annealed to a ^{32}P 5′-labeled 21-nt complementary oligonucleotide (5′-GCGGTCGAGTCTAGAGGAGCC-3′). This produces a primed-template with a 15 bases single-stranded 5′-tail. Reactions were carried out in 15 μl volumes containing 10 fmol DNA template, 20 mM Tris–HCl [pH 7.8], 1 mM DTT, 0.1 mg/ml bovine serum albumin, 10 mM $MgCl_2$, 10% glycerol, 2 mM ATP, 0.3 mM ddGTP and 3 mM dCTP. POLγA and POLγB were added as indicated in the figures and reactions were incubated at RT for 10 min before separation on a 6% Native PAGE gel in 0.5 × TBE for 35 min at 180 V. Bands were visualized by autoradiography.

For K_d analysis, band intensities representing unbound and bound DNA were quantified using Multi Gauge V3.0 software (Fujifilm Life Sciences). The fraction of bound DNA was determined from the background-subtracted signal intensities using the expression: bound/(bound+unbound). The fraction of DNA bound in each reaction was plotted versus the concentration of POLγA or POLγA-B2. Data were fit using the 'one site – specific binding' algorithm in Prism 8 (Graphpad Software) to obtain values for K_d.

Coupled exonuclease-polymerase assay

DNA polymerization and 3′-5′ exonuclease activity were assayed using the same primer-template as described above for electrophoresis mobility shift assay (EMSA). The reaction mixture contained 10 fmol of the DNA template, 25 mM Tris-HCl [pH 7.8], 10% glycerol, 1 mM DTT, 10 mM

$MgCl_2$, 100 μg/ml BSA, 60 fmol of POLγA, 120 fmol of POLγB and the indicated concentrations of the four dNTPs. The reaction was incubated at 37 °C for 15 min and stopped by the addition of 10 μl of TBE-UREA-sample buffer (BioRad). The samples were analysed on a 15% denaturing polyacrylamide gel in 1 × TBE buffer.

DNA synthesis on ssDNA template

A ^{32}P 5′-labeled 70-mer oligonucleotide [5′-42(T)-ATCTCA GCGATCTGTCTATTTCGTTCAT-3′] was hybridized to a single-stranded pBluescript SK(+). The template formed consists of a 42 nt single-stranded 5′-tail and a 28 bp duplex region. Reactions were carried out in 20 μl volumes containing 10 fmol template DNA, 25 mM Tris–HCl (pH 7.8), 1 mM DTT, 10 mM $MgCl_2$, 0.1 mg/ml BSA, 100 μM dATP, 100 of the four dNTPs, 2.5 pmol mtSSB, 150 fmol POLγA and 300 fmol POLγB. Reactions were incubated at 37 °C for the indicated times and stopped by the addition of 6 μl of stop buffer (90 mM EDTA, 6% SDS, 30% glycerol, 0.25% bromophenol blue and 0.25% xylene cyanol) and separated on a 0.9% agarose gel at 130V in 1 × TBE for 4 h.

Rolling circle *in vitro* replication assay

A ^{32}P 5′-labeled 70-mer oligonucleotide [5′-42(T)-ATCTCA GCGATCTGTCTATTTCGTTCAT-3′] was hybridized to a single-stranded pBluescript SK(+) followed by one cycle of polymerization using KOD polymerase (Novagen) to produce a ∼3-kb double-stranded template with a preformed replication fork. Reactions of 20 μl were carried out containing 10 fmol template DNA, 25 mM Tris–HCl (pH 7.8), 1 mM DTT, 10 mM $MgCl_2$, 0.1 mg/ml BSA, 4 mM ATP, 100 μM dATP, 100 μM dTTP, 100 μM dGTP, 10 μM dCTP, 2 μCi [α-^{32}P] dCTP, 2 pmol mtSSB, 200 fmol TWINKLE, 200 fmol POLγA and 500 fmol POLγB (or as indicated in the figure). Reactions were incubated at 37 °C for 60 min (or as indicated in the figure) and stopped with 6 μl alkaline stop buffer (18% [wt/vol] Ficoll, 300 mM NaOH, 60 mM EDTA [pH8], 0.15% [wt/vol] Bromocresol green and 0.35% [wt/vol] xylene cyanol). Products were run in 0.8% alkaline agarose gels and visualized by autoradiography.

Incorporation of [α-^{32}P]-dCTP was measured by spotting 5 μl aliquots of the reaction mixture (after the indicated time points at 37°C) on Hybond N+ membrane strips (GE Healthcare Lifesciences). The membranes were washed (3 × with 2 × SSC and 1 × with 95% EtOH) and the remaining activity was quantified using Multi Gauge V3.0 software (Fujifilm Life Sciences). A dilution series of known specific activity of [α-^{32}P]-dCTP was used as a standard.

Thermofluor assay

The fluorescent dye Sypro Orange (Invitrogen) was used to monitor the temperature-induced unfolding of WT and mutant POLγA as previously described (31). Briefly, WT and mutant proteins were set up in 96-well PCR plates at a final concentration of 1.6 μM protein and 5 × dye in assay buffer (50 mM Tris–HCl pH 7.8, 10 mM DTT, 50 mM $MgCl_2$ and 5 mM ATP). Differential scanning fluorimetry was performed in a C1000 Thermal Cycler using the CFX96 real time software (BioRad). Scans were recorded using the HEX emission filter (560–580 nm) between 4 and 95 °C in 0.5 °C increments with a 5 s equilibration time. The melting temperature (T_m) was determined from the first derivative of a plot of fluorescence intensity versus temperature (32). The standard error was calculated from three independent measurements.

LONP1 proteolysis assay

Protease activity of purified LONP1 on POLγA was measured in a 15 μl reaction volumes containing 0.5 μg of LONP1 WT and 0.55 μg of POLγA (in presence or absence of 0.22 μg of POLγB). When having both POLγA and POLγB in the same reaction, a preincubation in ice for 10 min is made before adding LONP1 to the reaction. Samples were incubated at 37 °C for 0–90 min in a buffer containing 50 mM Tris–HCl pH 8.0, 10 mM $MgCl_2$, 0.1 mg/ml BSA, 2 mM ATP and 1 mM DTT and the reactions were stopped by addition of Laemli sample buffer (BioRad). Samples were run on precast 4–20% gradient SDS-PAGE gels (BioRad, 567–8094) and visualized using ImageLab™ (BioRad) to detect proteolytic activity on POLγA. Band intensities were measured with ImageLab™ (BioRad) and calculations were made in order to provide % remaining POLγA-values. Reactions and calculations were made in triplicate and SD was calculated.

Gel filtration analysis

Complex formation between POLγA and POLγB was tested by size-exclusion chromatography using a Superose 6 Increase 10/300 column (GE Healthcare) connected to an ÄKTA Purifier (GE Healthcare). The column was equilibrated in buffer D (25 mM Tris–HCl, pH 7.8, 10% glycerol, 1 mM DTT, 0.5 M NaCl, 10 mM $MgCl_2$). Equal amounts (1 nmol) of POLγA and POLγB (calculated as a dimer) were pre-incubated in buffer D for 10 min on ice before injection. Samples (200 μl) were injected onto the column through a 200 μl loop and run at 1 ml/min. Fractions of 250 μl were collected and analyzed on a precast 4–20% gradient SDS-PAGE gel and visualized using ImageLab™ (BioRad). A size calibration curve was previously prepared using thyroglobulin (670 kDa), c-globulin (158 kDa), ovalbumin (44 kDa), myoglobin (17 kDa) and vitamin B12 (1.35 kDa) according to the manufacturer's instructions (BioRad, 151–1901).

To analyze the LONP1^{S855A}-POLγA interaction, a home-made gel filtration column (0.5 cm x 30 cm) was prepared using Bio-Gel agarose with a bead size of 75–150 μm (BioRad, 151–0440) and calibrated using a gel filtration standard (BioRad, 151–1901). Preincubation of the proteolytic mutant of LONP1 with POLγA in the presence of 2 mM ATP and 10 mM $MgCl_2$ at 37 °C for 10 min allowed the formation of the complex that was later injected into the column and eluted in 1 CV of buffer D. Fractions of 200 μl were collected and analyzed in a precast 4–20% gradient SDS-PAGE gel and visualized using ImageLab™ (BioRad).

Statistical analysis

All numerical data are expressed as mean ± SEM unless otherwise stated. A two tailed Student's *t*-test was used to assess statistical significance (see figure legends for details) in two groups comparisons. Two-way ANOVA test with Tukey's correction was used for multiple comparisons. Differences were considered statistically significant for $P < 0.05$. Animals were randomized in treated and untreated groups. No blinding to the operator was used.

RESULTS

Generation and characterization of *Polg*$^{A449T/A449T}$ mutant mice

To investigate the molecular pathogenesis of *POLG*-related disorders, we generated a *Polg*$^{A449T/A449T}$ homozygous knockin mouse, corresponding to the human A467T mutation, by CRISPR/Cas9 technology (Supplementary Figure S1). Three-month-old *Polg*$^{A449T/A449T}$ homozygous animals did not show any gross phenotype compared to WT littermates, including similar body weight curve and rotarod performance (not shown). However, a 19.6% ($P < 0.05$) reduction in treadmill motor endurance was detected (Figure 1A). Although whole body metabolism was similar in KI and controls by CLAMS analysis, a 41% ($P < 0.05$) reduction in spontaneous rearing movements was observed in *Polg*$^{A449T/A449T}$ mutants (Figure 1B and C; Supplementary Figure S2). Aged, 1-year-old *Polg*$^{A449T/A449T}$ homozygous animals were very similar to the 3-month-old mice ruling out a late onset phenotype (Supplementary Figure S3A and B). Post-mortem hematoxylin and eosin staining at both ages did not show any gross abnormality in any tissue (Supplementary Figure S4). We monitored the *Polg*$^{A449T/A449T}$ and WT littermates up to 2 years of age, but neither reduction of the lifespan nor the presence of obvious age-related phenotypes was observed. Therefore, we focused our analysis on 3-month-old animals, unless otherwise stated.

POLγA is reduced in *Polg*$^{A449T/A449T}$ tissues

We analysed the effects of the A449T mutation on POLγA and POLγB protein levels. Immunoblotting revealed a strong reduction of POLγA^{A449T} amount, as low as 50%, in all tissues examined, including liver, SKM, brain, kidney and heart (Figure 2A and B). In contrast, POLγB levels were unchanged in most tissues, albeit a mild upregulation and downregulation in brain and heart, respectively, was observed (Figure 2A–C). Analysis of the corresponding mRNAs showed no significant changes of *Polg* or *Polg2* transcripts in both liver and SKM of *Polg*$^{A449T/A449T}$ compared to control littermates (Figure 2D and E), suggesting post-translational instability of the mutant protein.

Reduced mtDNA content and impaired replication in *Polg*$^{A449T/A449T}$ tissues and MEFs

Since mutations in *POLG* are associated with mtDNA instability in human patients, we next investigated mtDNA content and integrity in several tissues, including liver, SKM, brain, kidney and heart from both *Polg*$^{A449T/A449T}$ versus WT littermates (Figure 3A). MtDNA copy number was significantly reduced in the SKM of 3-month-old *Polg*$^{A449T/A449T}$ (80 ± 4%, $P < 0.01$) compared to WT littermates without accumulation of multiple deletions (Figure 3B and Supplementary Figure S5A–C). No difference in mitochondrial transcripts and OXPHOS activities were detected between *Polg*$^{A449T/A449T}$ versus WT littermates in liver and SKM (Supplementary Figure S5D–J). Multiple deletions were also not detected in tissues of 1-year-old *Polg*$^{A449T/A449T}$ homozygous animals and mtDNA quantifications were very similar to that of the 3-month-old mice, except that in addition to SKM, a mild decrease in mtDNA copy number was also observed in kidney (79 ± 6%, $P < 0.01$) and heart (87 ± 3%, $P < 0.01$) (Supplementary Figure S3C–H).

To investigate in detail the effects on mtDNA replication, we generated mouse embryonic fibroblasts (MEFs) from *Polg*$^{A449T/A449T}$ and WT cells. The mtDNA content was similar in the two genotypes (Supplementary Figure S5K). We then investigated mtDNA replication in MEFs, using 5-ethynyl-2′-deoxyuridine (EdU) staining in conjunction with an anti-DNA antibody to label replicating and total mtDNA. Interestingly, we observed a significantly increased fraction of replicating mtDNA molecules in *Polg*$^{A449T/A449T}$ versus WT MEFs (Figure 3C–F), indicating that more mtDNA foci were engaged in replication. Next, we used ethidium bromide (EtBr) to deplete mtDNA content, and found that after removal of EtBr, mtDNA content recovered to pre-treatment values within 3 days in WT MEFs, whereas no recovery at all was observed in the mutant cells (Figure 3G), strongly indicating severely impaired mtDNA replication in stress conditions of *Polg*$^{A449T/A449T}$ mouse mitochondria.

Given the mild reduction in mtDNA copy number in the mutant mice, we decided to challenge them with a single injection of carbon tetrachloride (CCl_4), which induces acute liver damage, triggering liver cell division to repopulate the necrotic areas. Two days after the injection, both WT and *Polg*$^{A449T/A449T}$ showed extensive areas of necrosis (∼35% of the liver), which was reduced to 6 ± 0.46% in WT mice after 4 days, whereas it was still above 10% in *Polg*$^{A449T/A449T}$ mice (10 ± 1.15%, $P < 0.05$) (Figure 3H and I). This result clearly indicates that cell replication is impaired in *Polg*$^{A449T/A449T}$, likely due to the lack of bioenergetic supply by impaired mitochondria in stress conditions. Since the antiepileptic drug valproic acid (VPA) is known to induce acute liver failure in patients with the A467T mutation in POLγA (33,34), we treated our mice with VPA by daily oral gavage (300 mg/kg) for one week or in food pellets (1.5% VPA) for 2 months. Both WT and *Polg*$^{A449T/A449T}$ did not show any sign of hepatic failure or histological damage.

Polg$^{A449T/A449T}$ mitochondria have reduced 7S DNA and accumulate replication intermediates

We then investigated mtDNA replication in the tissues of the mutant and control mice by Southern blot. Normally, about 95% of all replication events are prematurely terminated, generating a 650 nucleotide-long molecule, called 7S DNA (35–37). In *Polg*$^{A449T/A449T}$ but not in WT littermate, the 7S DNA levels were significantly reduced in SKM and

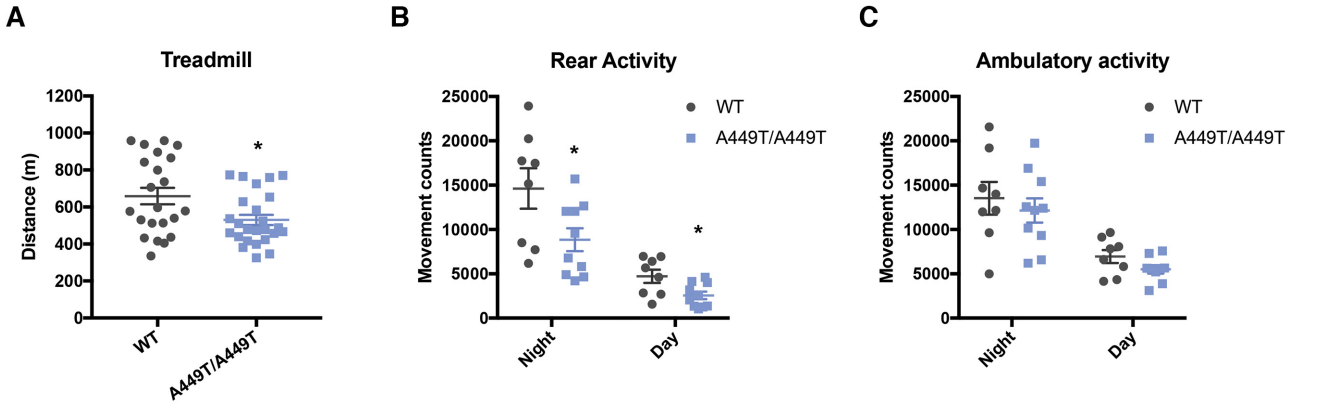

Figure 1. Characterization of the clinical phenotype of $Polg^{A449T/A449T}$ mice. (**A**) Distance run in metres by 3-month-old WT and $Polg^{A449T/A449T}$ animals on the treadmill. Data are presented as mean ± SEM. $*P < 0.05$; Student's *t*-test. Each symbol represents a biological replicate. (**B**) Spontaneous rear activity (vertical movement counts) of 3-month-old WT and $Polg^{A449T/A449T}$ animals measured in the CLAMS™ system. Data are presented as mean ± SEM. Two tailed unpaired Student's *t*-test: $*P < 0.05$; each symbol represents a biological replicate. (**C**) Spontaneous ambulatory activity (horizontal movement counts) of 3-month-old WT and $Polg^{A449T/A449T}$ animals measured in the CLAMS™ system. Data are presented as mean ± SEM. Student's *t*-test. Each symbol represents a biological replicate.

kidney, and a similar trend was also present in the other analysed tissues, except for the heart, (Figure 4A-B and Supplementary Figure S6A-C). These results suggest compensatory mtDNA replication in knockin mice versus WT littermates.

To better investigate the mechanistic details of mtDNA replication, we then performed *in organello* replication experiments in isolated liver mitochondria (Figure 4C), by pulse-labeling with α-^{32}P-dATP. Although no obvious differences were detected in mtDNA replication rates between $Polg^{A449T/A449T}$ and WT mice (Figure 4C), the signal due to long but incomplete mtDNA molecules was much more intense in the *Polg* mutant compared to WT samples, thus suggesting accumulation of replication intermediates (RIs) in the mutant versus controls. Accordingly, we applied two-dimension agarose gel electrophoresis (2D-AGE), which resolves DNA molecules based on size and shape, allowing a snapshot of the RIs. Notably, $Polg^{A449T/A449T}$ mice displayed an overall accumulation of the different types of RIs compared to WT animals (Figure 4D and Supplementary Figure S6D–F), revealing abnormal replication of $Polg^{A449T/A449T}$ mainly due to generalized replication fork stalling. These results are concordant with those found in MEFs (Figure 3C–F). These novel data clearly demonstrate that the A449T mutation impairs mtDNA replication in both cultured cells and *in vivo*.

POLγA^{A449T} protein has reduced affinity for DNA and polymerase activity, which are partially rescued by POLγB subunit

To further document the stalling phenotype of the A449T mutant *in vitro*, we expressed and purified both human (h) and mouse (m) WT and mutant POLγA as recombinant proteins. First, we used an EMSA to measure the binding of mPOLγA to a primed DNA template. When alone, mPOLγA^{A449T} bound DNA ≈ 3.4 times less than mPOLγA^{WT} (Figure 5A and Supplementary Figure S7A) and remained 1.75 times lower than the WT also after the addition of POLγB (Figure 5B and Supplementary Figure S7B).

Next, we investigated mPOLγA activities using a short DNA template annealed to a radioactively labeled primer. By performing the experiment across a range of dNTP concentrations, we could analyze both polymerase and exonuclease function. The exonuclease activity can digest the labeled primer, whereas the polymerase activity can elongate the primer and synthesize an additional short, 15 nucleotide-stretch of DNA. As expected, at lower dNTP levels, mPOLγA^{WT} displayed 3′-5′ exonuclease activity, but at higher concentrations, it switched to polymerase activity (Figure 5C). Addition of mPOLγB reduced exonuclease activity and favored DNA synthesis even at lower dNTP concentrations (Figure 5D). The mutant mPOLγA^{A449T} was completely inactive in isolation, most likely due to its inability to efficiently bind primed DNA (Figure 5C). Nevertheless, addition of mPOLγB restored the polymerase activities of mPOLγA^{A449T}, to levels similar to those observed with mPOLγA^{WT} (Figure 5D), whereas exonuclease activity was reduced also in mPOLγA^{WT} as a consequence of predominant polymerase activity measured *in vitro* (Figure 5D).

To further challenge the system, we performed DNA synthesis assay using a long circular ssDNA template of 3000 nt (Figure 5E). mPOLγA^{A449T} displayed a clearly slower DNA synthesis rate compared to the mPOLγA^{WT}, even in the presence of the mPOLγB subunit (Figure 5F). To monitor the effects of the A449T mutation on replication of dsDNA, we used a template containing a ∼4 kb long dsDNA region with a free 3′-end acting as a primer (Figure 5G). Addition of the TWINKLE DNA helicase was required to unwind the DNA and the reaction was stimulated by mtSSB (Figure 5G). This reaction is absolutely dependent on POLγB and once initiated, very long stretches of DNA can be formed. In this rolling circle replication assay, mPOLγA^{A449T} showed reduced polymerase DNA synthesis rate (Figure 5H) compared to mPOLγA^{WT}, at all concentrations tested (Supplementary Figure S7C), demonstrating

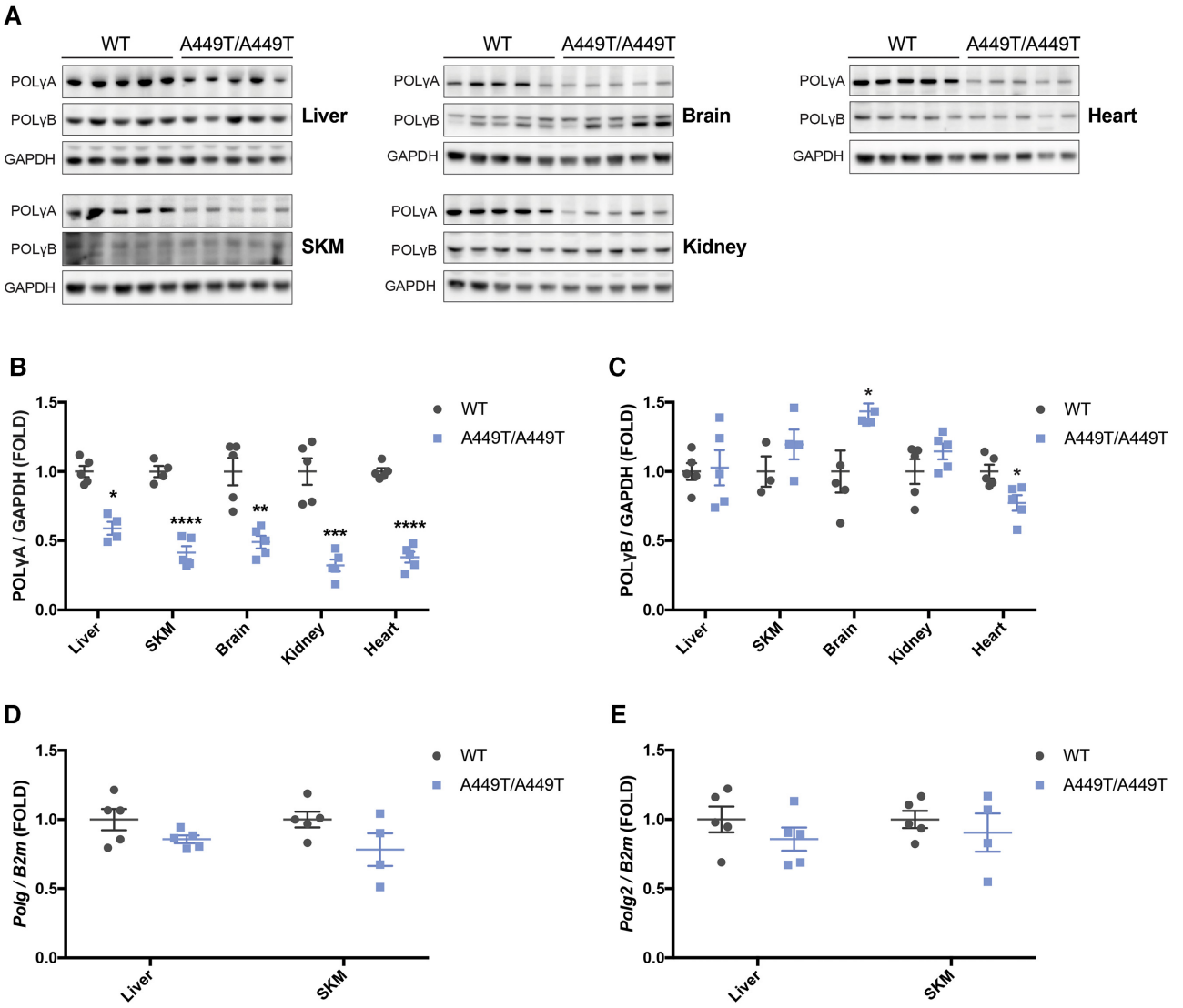

Figure 2. Characterization of POLγA and POLγB levels in tissues of *Polg*$^{A449T/A449T}$ mice. (**A**) Western blot analysis of steady-state levels of POLγA and POLγB in liver, SKM, kidney, brain and heart of WT and *Polg*$^{A449T/A449T}$ animals. The lower band in the brain is unspecific. GAPDH was used as loading control. Each lane represents a biological replicate. (**B** and **C**) Quantification of (A). POLγA (B) and POLγB (C) levels were normalized to GAPDH and presented as FOLD change from WT animals. Data are presented as mean ± SEM. Two tailed unpaired Student's *t*-test: $*P < 0.05$; $**P < 0.01$; $***P < 0.001$; $****P < 0.0001$. Each symbol represents a biological replicate. (**D** and **E**) Real-time qRT-PCR quantification of the transcripts *Polg* (D) and *Polg2* (E), normalized to *B2m*, in liver and SKM of WT and *Polg*$^{A449T/A449T}$ animals. Data are presented as mean ± SEM. Two tailed unpaired Student's *t*-test: non significant. Each symbol represents a biological replicate.

that mPOLγA^{A449T} has reduced polymerase activity. This *in vitro* result is in perfect agreement with the stalling phenotype seen *in vivo*. A similar effect was obtained with the hPOLγA^{A467T} (Figure 5I).

Analysis of incorporated radiolabeled nucleotides over time indicated that the *in vitro* replication rates with 10 μM dNTPs, were reduced to about 60% for mPOLγA^{A449T} compared to mPOLγA^{WT} (3.5 fmol/min versus 5.5 fmol/min) (Supplementary Figure S7D and E). Interestingly, the reduction was more pronounced with hPOLγA^{A467T} compared to hPOLγA^{WT} (1.4 versus 5.3 fmol/min), than for the mouse equivalents, which could explain the more severe phenotype observed in patients (Supplementary Figure S7D and E).

POLγA is unstable in absence of POLγB

The amount of mPOLγA^{A449T} was reduced in the *Polg*$^{A449T/A449T}$ mice, which could also contribute to impaired mtDNA replication. To better understand the impact of the A449T mutation on protein stability, we performed a thermofluor stability assay and monitored temperature-induced unfolding of mPOLγA^{WT} and mPOLγA^{A449T}, both in the absence and in the presence of mPOLγB (Figure 6A and B). The stability assay revealed no major differences in the fluorescence profile between mPOLγA^{WT} and mPOLγA^{A449T} from 37 °C upwards, but the fluorescence signal of mPOLγA^{A449T} was already higher than the WT at 25 °C, clearly indicating that the mutant protein was already partially unfolded even at

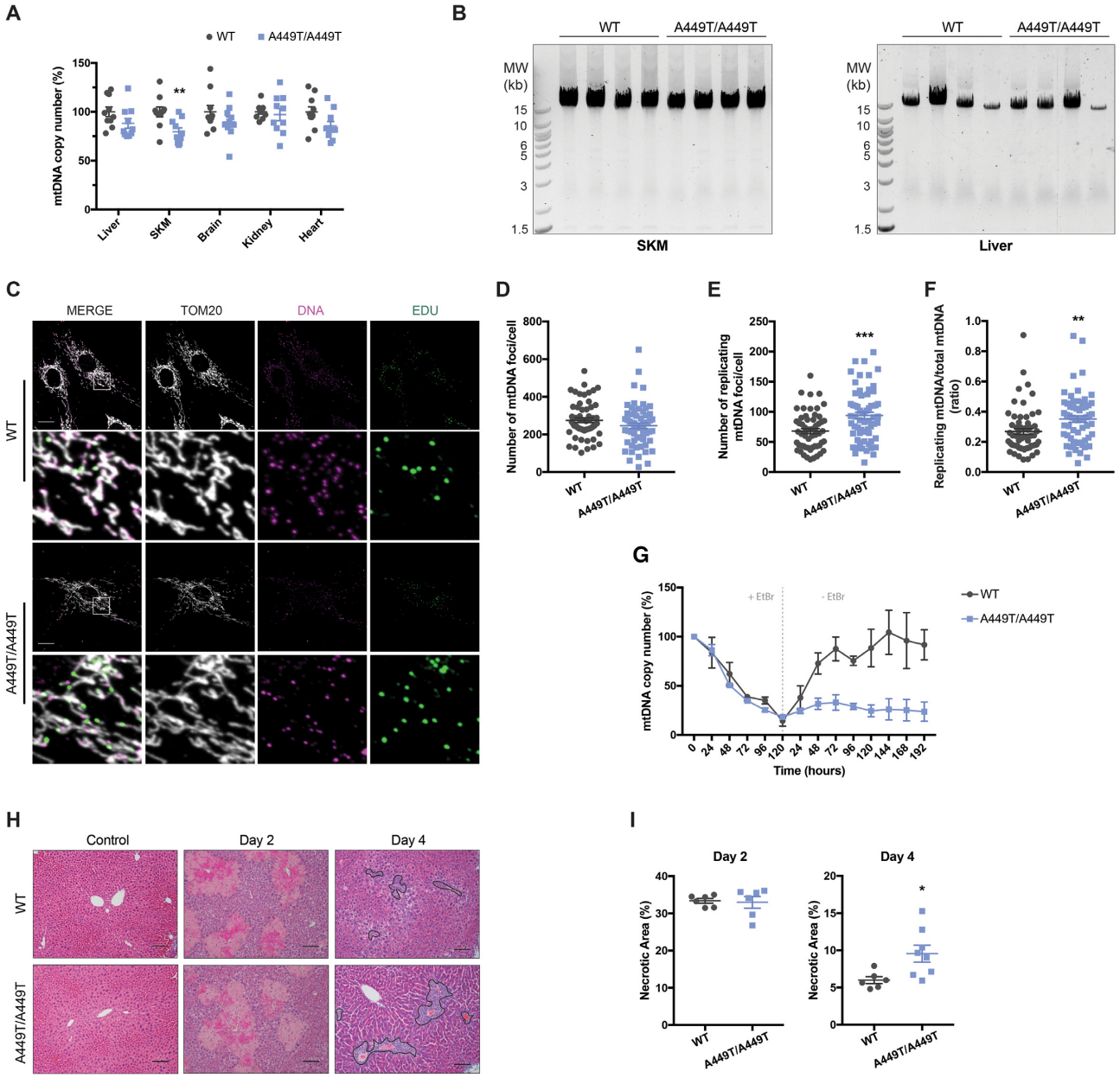

Figure 3. Characterization of the molecular phenotype of *Polg*$^{A449T/A449T}$ mice. (**A**) Real-time qPCR quantification of mtDNA content in liver, SKM, kidney, brain and heart of WT and *Polg*$^{A449T/A449T}$ animals. Data are presented as mean ± SEM. Two tailed unpaired Student's *t*-test: $^{**}P < 0.01$. Each symbol represents a biological replicate. (**B**) Long-range PCR performed in DNA isolated from SKM and liver of WT and *Polg*$^{A449T/A449T}$ animals. Primers amplifying a fragment of 15 781 bp of the mtDNA. The bands were visualized by SYBR™ safe staining. Each lane represents a biological replicate. (**C**) Representative confocal images of mitochondria, DNA and replicating mtDNA (EdU) from WT and *Polg*$^{A449T/A449T}$ MEFs. Mitochondria and mtDNA were labeled using anti-TOM20 and anti-DNA antibodies, respectively. Replicating DNA was visualized in fixed cells after incubation with 50 μM EdU for 1 h. Scale bar 20 μm. (**D**) Quantification of total mtDNA from (C). Data are presented as mean ± SEM. Two tailed unpaired Student's *t*-test: P = non significant. Each symbol represents individual cells ($n = 60$) from three independent experiments. (**E**) Quantification of mitochondrial EdU positive foci from (C). Data are presented as mean ± SEM. Two tailed unpaired Student's *t*-test: $^{***}P < 0.001$. Each symbol represents individual cells ($n = 60$) from three independent experiments. (**F**) Ratio of the mitochondrial replicating mtDNA/total mtDNA. Data are presented as mean ± SEM. Two tailed unpaired Student's *t*-test: $^{**}P < 0.01$. Each symbol represents individual cells ($n = 60$) from three independent experiments. (**G**) Real-time qPCR quantification of mtDNA content in WT and *Polg*$^{A449T/A449T}$ MEFs during ethidium bromide-mediated depletion and then recovery of mtDNA. Data are presented as mtDNA percentage (%) of untreated cells of each genotype. Data are presented as mean ± SEM ($n = 3$). (**H**) Representative H&E staining of liver tissue sections of WT (top) and *Polg*$^{A449T/A449T}$ (bottom) animals with a single injection of CCl_4. Two days after injection (middle), 4 days after injection (right) and control/non-injected mice (left). Note the necrotic areas around the central veins (highlighted with black lines at day 4). Scale bar 100 μm. (**I**) Quantification of necrotic areas (H) as percentage (%) of the total section area, 2 and 4 days after a single injection of CCl_4. Data are presented as mean ± SEM. Two tailed unpaired Student's *t*-test: $^{*}P < 0.05$. Each symbol represents a biological replicate.

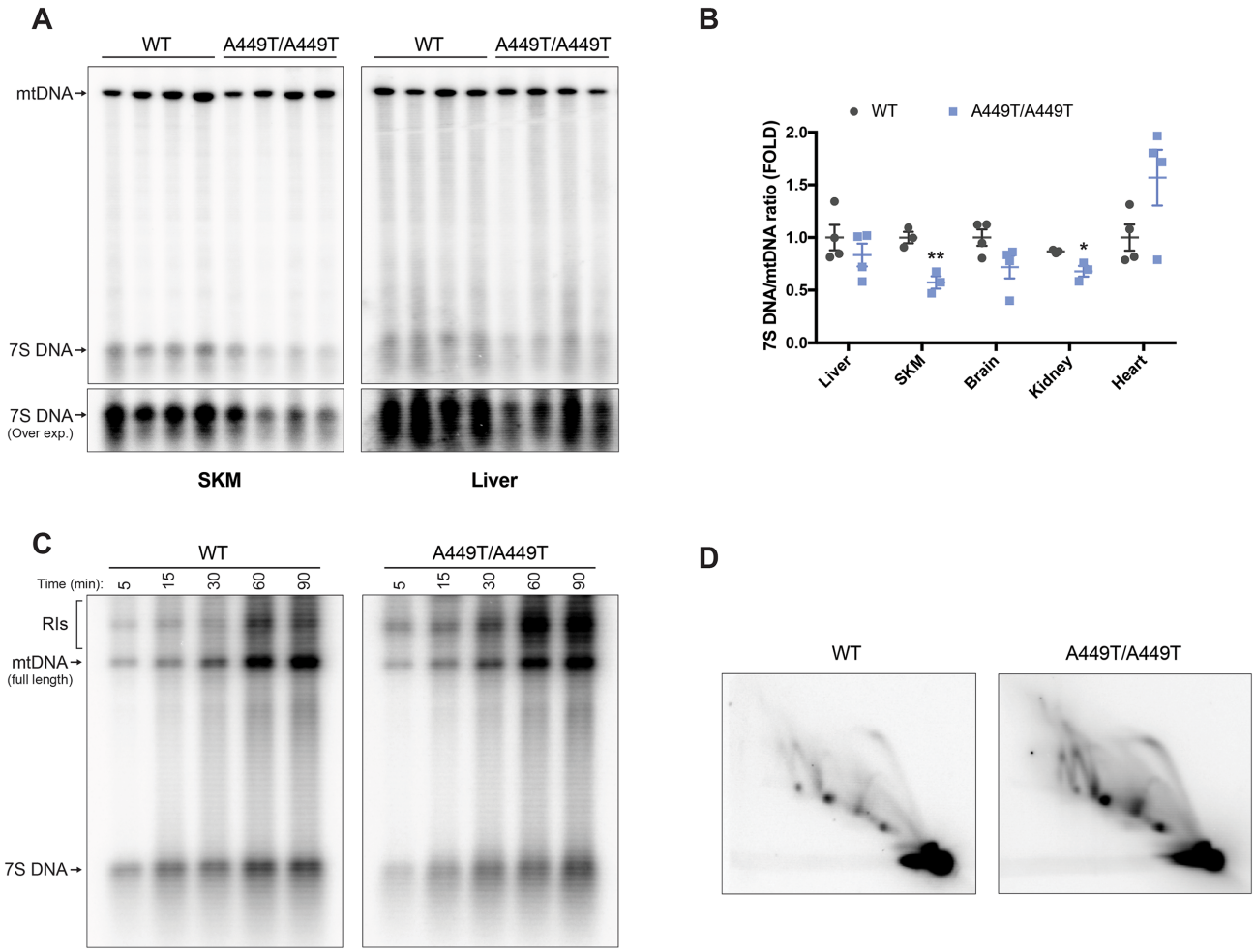

Figure 4. Molecular analysis of mtDNA replication in *Polg*$^{A449T/A449T}$ mitochondria. (**A**) Southern blot analysis of BlpI-digested mtDNA and 7S DNA from SKM and liver of WT and *Polg*$^{A449T/A449T}$ animals. (**B**) Quantification of the Southern blots presented in panel (A) and Supplementary Figure S6A–C. 7S DNA levels were normalized to linearized full length mtDNA and presented as FOLD change from WT animals. Data are presented as mean ± SEM. Two tailed unpaired Student's *t*-test: **P* <0.05; ***P* <0.01. Each symbol represents a biological replicate. (**C**) Time course of *de novo* DNA synthesis of mtDNA, 7S DNA and RIs in liver-isolated mitochondria of WT and *Polg*$^{A449T/A449T}$ animals. Brackets indicate mtDNA replication intermediates (RIs). Pulse-labeling time (min) is indicated on the top. (**D**) Analysis of the mtDNA RIs in the liver of WT and *Polg*$^{A449T/A449T}$ mice, resolved by 2D-AGE and followed by southern blot visualization. DNA was digested with the BclI restriction enzyme. For probe and restrictions sites location, schematic representation and quantification of the different types of RIs, please refer to (Supplemental Figure S6D-F).

<37 °C temperatures (Figure 6A and B). Interestingly, the presence of the mPOLγB had a dramatic stabilizing effect, by increasing the unfolding temperature of about 10 °C for both proteins (Figure 6A and B). These data suggest that POLγA^{WT} is also partially unstable in the absence of POLγB. Accordingly, a recent report demonstrated that human POLγB-knockout cells showed severe decrease in POLγA levels (38).

We hypothesized that the A449T mutation could impair interactions with mPOLγB and thus destabilize mPOLγA^{A449T}. The A449 (mouse)/A467 (human) residue is located in the thumb helix that forms contacts with POLγB. The mutation disrupts the local hydrophobic environment formed by L466 and L602. As a consequence, there is a slight spatial shift of the thumb domain, which could potentially disturb binding to POLγB. (Supplementary Figure S8A) (39). To address this possibility, we investigated mPOLγA^{A449T} interactions with mPOLγB by performing size-exclusion chromatography. At 1:1 molar ratio of mPOLγA and mPOLγB (calculated as a dimer), mPOLγ^{WT} and mPOLγB migrated as a single peak, corresponding to a stable complex between the two proteins (Figure 6C), as confirmed by SDS-PAGE (Figure 6D). In contrast, mPOLγA^{A449T} and mPOLγB showed an additional peak, corresponding to unbound mPOLγB (Figure 6C and E). The resolution of the chromatography cannot separate free POLγA from the POLγ holoenzyme. Thus, the A449T mutation significantly reduces the interaction between POLγA and POLγB subunits. This observation is in agreement with the data for hPOLγA^{A467T} (11).

POLγB protects POLγA against LONP1 degradation

Next, we investigated if free, partially unfolded POLγA could be a target for protein degradation. The LONP1 protease degrades misfolded proteins in mitochondria and has

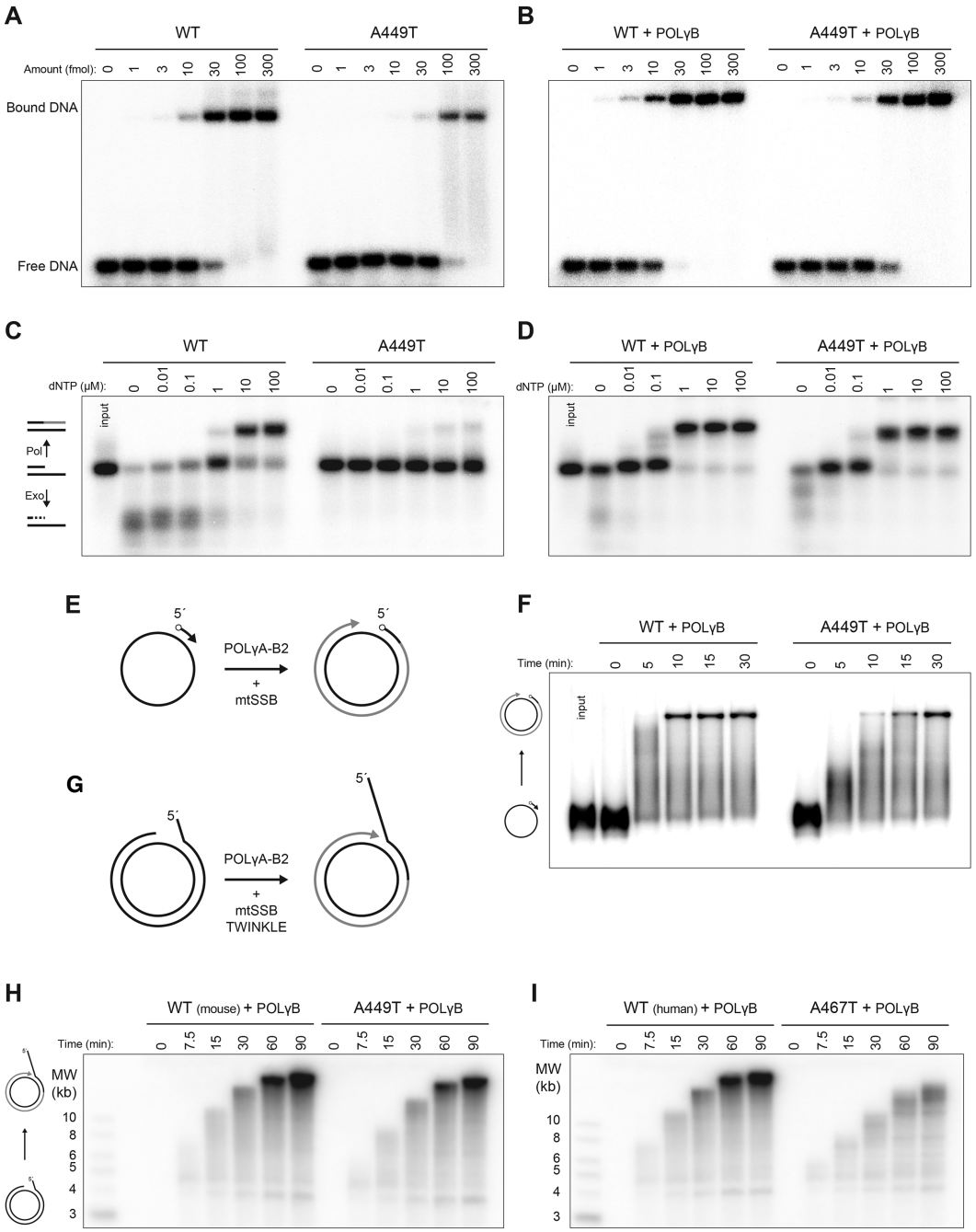

Figure 5. *In vitro* characterization of POLγA^{A449T} mutant protein. (**A**) Electrophoretic mobility assays using mPOLγA^{WT} and mutant mPOLγA^{A449T} to estimate affinity to a DNA template. For K_d(DNA) calculations please refer to Supplemental Figure S7A. Each lane contains 10 fmol of DNA substrate and the indicated amounts of POLγA on the top. (**B**) Electrophoretic mobility assays using mPOLγA^{WT} and mutant mPOLγA^{A449T} with addition of mPOLγB to estimate affinity to a DNA template. For K_d(DNA) calculations please refer to Supplementary Figure S7B. Each lane contains 10 fmol of DNA substrate and the indicated amounts of POLγ holoenzyme on the top. (**C**) Coupled exonuclease–polymerase assay using mPOLγA^{WT} and mutant mPOLγA^{A449T} across increasing concentrations of dNTPs using a short DNA template. A schematic representation of the assay is presented on the left. (**D**) Coupled exonuclease–polymerase assay using mPOLγA^{WT} and mutant mPOLγA^{A449T} with addition of mPOLγB, across increasing concentrations of dNTPs using a short DNA template. (**E**) Schematic representation of the second strand synthesis assay. This assay evaluates the ability of polymerise long stretches of DNA by synthesizing the second strand of a single-stranded template hybridized with a 5' radiolabeled primer. MtSSB is added in the reaction. (**F**) Second strand synthesis assay using mWT and mutant mPOLγA^{A449T} to assess polymerase activity using longer DNA templates. The reactions include POLγA-B2 and mtSSB and were incubated for the indicated times on top of the blot. (**G**) Schematic representation of the rolling circle *in vitro* replication assay. The template consists of an incomplete double stranded DNA template with a mismatch on the 5' of the incomplete strand. In the presence of TWINKLE and mtSSB, POLγA-B2 can polymerase long stretches of DNA using the 3'-end of the incomplete strand. (**H**) Rolling circle *in vitro* replication assay using mPOLγA^{WT} and mutant mPOLγA^{A449T} to assess polymerase activity in the context of the minimal mitochondrial replisome, which includes POLγ holoenzyme WT or mutant, TWINKLE and mtSSB. The reactions were incubated for the indicated times (top). (**I**) Rolling circle *in vitro* replication assay using human versions of hPOLγA^{WT} and mutant hPOLγA^{A467T} to assess polymerase activity in the context of the minimal mitochondrial replisome (POLγ holoenzyme WT or mutant, TWINKLE and mtSSB). The reactions were incubated for the indicated times (top).

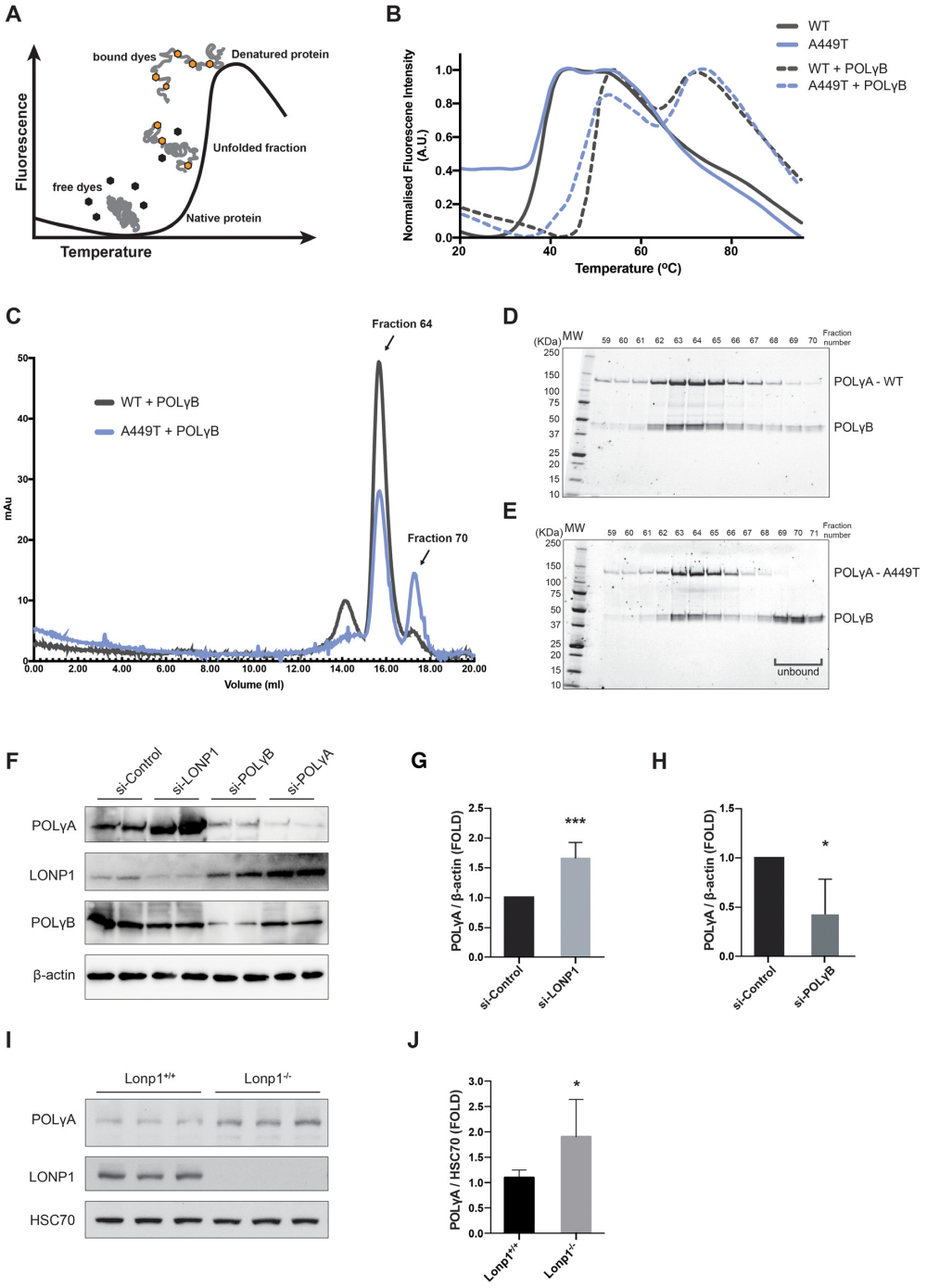

Figure 6. Stability of POLγA^{A449T} mutant protein *in vitro* and *in vivo*. (**A**) Schematic representation of a typical thermofluor stability assay. This assay uses a fluorescent dye, SYPRO Orange, to monitor the temperature-induced unfolding of proteins. When the temperature starts to rise and unfold the protein, the SYPRO Orange dye fluoresces by binding to exposed hydrophobic patches. (**B**) Thermofluor stability assay to evaluate thermostability of mPOLγA^{WT} (black) and mPOLγA^{A449T} (blue), in absence (solid line) or presence (dashed line) of mPOLγB. (**C**) Size-exclusion chromatogram of mPOLγA^{WT} (black line) and mPOLγA^{A449T} (blue line) in presence of mPOLγB, to evaluate interaction between POLγA and POLγB. (**D**) SDS-PAGE of the selected peak fractions from (C) of mPOLγA^{WT} and mPOLγB. (**E**) SDS-PAGE of the selected peak fractions from (C) of mPOLγA^{A449T} and mPOLγB. Note the brackets highlighting unbound POLγB (free from POLγA^{A449T}). (**F**) Western blot analysis of steady-state levels of POLγA, LONP1 and POLγB upon siRNA-mediated knockdown of LONP1, POLγB and POLγA, in HeLa cells. ß-actin was used as loading control. (**G**) Quantification of POLγA levels upon siRNA-mediated knockdown of LONP1 (F). POLγA levels were normalized to ß-actin and presented as FOLD change from cells treated with control siRNA. Data are presented as mean ± SEM. Two tailed unpaired Student's *t*-test: $***P < 0.001$. ($n = 3$). (**H**) Quantification of POLγA levels upon siRNA-mediated knockdown of POLγB (F). POLγA levels were normalized to ß-actin and presented as fold change from cells treated with control siRNA. Data are presented as mean ± SEM. Two tailed unpaired Student's *t*-test: $***P < 0.001$. ($n = 3$). (**I**) Western blot analysis of steady-state levels of POLγA in heart of *Lonp1*$^{+/+}$ and *Lonp1*$^{-/-}$ animals. An anti-LONP1 antibody was used to confirm gene knockout and HSC70 was used as loading control. (**J**) Quantification of POLγA levels in heart of *Lonp1*$^{+/+}$ and *Lonp1*$^{-/-}$ animals (I). POLγA levels were normalized to HSC70 and presented as fold change from *Lonp1*$^{+/+}$. Data are presented as mean ± SEM. Two tailed unpaired Student's *t*-test: $*P < 0.05$. ($n = 6$).

previously been linked to regulation of mtDNA copy number (40). We decided to investigate if POLγA was a target for LONP1.

We first used siRNA interference against LONP1, POLγA and POLγB in HeLa cells. Interestingly, LONP1 knockdown caused a robust increase in POLγA levels (Figure 6F and G), whereas POLγB was unaffected (Figure 6F), supporting the idea that POLγA, but not POLγB, is a specific target for LONP1 degradation. In agreement with a stabilizing effect of POLγB, knockdown of *Polg2* mRNA also caused a reduction of POLγA levels (Figure 6F and H). Both POLγB and POLγA knockdown resulted in an increase of LONP1 (Figure 6F). We also evaluated the steady state levels of POLγA in a heart-specific *Lonp1*$^{-/-}$ mouse model (6I and 6J). Notably, POLγA levels were increased in heart samples of *Lonp1*$^{-/-}$ compared to control littermates. Collectively, these results support that LONP1 specifically targets POLγA both in cells and *in vivo*.

To investigate if POLγA is a direct target for LONP1 degradation, we performed a size-exclusion chromatography with recombinant protein to assess if human POLγA can form a complex with LONP1. To ensure that POLγA was not degraded by LONP1 during the experiment, we used the mutant LONP1^{S855A}, which traps substrates without degrading them (41). As shown in Figure 7A, we observed a co-elution of LONP1^{S855A} and hPOLγA, revealing an interaction between these two proteins.

We also monitored LONP1-dependent degradation of POLγA and POLγB *in vitro*. We followed the reactions over time and used another well-characterized LONP1 substrate, TFAM, as a positive control (21,42). The TFAM levels were reduced by 50% in about 3 min (Figure 7B). Mouse POLγB was not degraded by LONP1, confirming that the accessory subunit is not a substrate of the protease (Figure 7C, lanes 7–10). In contrast, both isolated mPOLγA^{WT} and mPOLγA^{A449T} were efficiently degraded, with a 50% reduction in about 20 min (Figure 7C, lanes 2–5, 7D, lanes 2–5 and E). The slower degradation time compared to TFAM could in part be explained by the size difference between the two substrates, with POLγA being about 6-fold larger. LONP1 is an ATP-dependent enzyme, and no degradation of POLγA was therefore observed in the absence of ATP (Figure 7C, lanes 1, 6 and 11).

Next, we examined POLγA in complex with POLγB. Interestingly, the presence of mPOLγB completely blocked mPOLγA^{wt} degradation (Figure 7C, lanes 12–15 and Figure 7E). In contrast, mPOLγB was unable to efficiently block degradation of mPOLγA^{A449T} and the levels of the mutant protein decreased significantly over the time of the experiment (Figure 7D, compare lanes 7–10 with 12–15 and Figure 7E). We also used the human WT and A467T mutant versions of POLγA, and obtained similar results (Figure 7F, G and H). We conclude that the impaired interaction between POLγB and mPOLγA^{A449T} leads to increased LONP1-dependent degradation of mPOLγA^{A449T}. This observation could explain the lower levels of mPOLγA^{A449T} observed *in vivo*.

To validate our model, we also analyzed two additional POLγA mutations: the mouse version of POLγA^{W748S} (POLγA^{W726S}), which also displays reduced interactions with POLγB (Supplementary Figure S9A–C), and human POLγA^{D274A}, which has no effect on POLγB interactions (43). As expected, mPOLγA^{W726S} but not hPOLγA^{D274A} was degraded in presence of POLγB (Supplementary Figure S9D–F).

Our observations *in vitro* implied that the POLγB dimer must be present in at least stoichiometric amounts *in vivo* to prevent POLγA degradation. To determine the *in vivo* ratio of the two proteins, we performed quantitative immunoblotting using polyclonal antibodies against the POLγA and POLγB in various mouse tissues (kidney, liver, brain, SKM and heart) and human HeLa cells. Protein levels were determined by comparison with known amounts of recombinant POLγA and POLγB. As predicted, the levels of the POLγB dimer was higher than POLγA in all cell types investigated. The ratio varied between 4:1 and 15:1 of the POLγB dimer relative POLγA (Supplementary Figure S8B–E). Overall, these data provide evidence that POLγB affects POLγA folding and protects the protein from degradation. Our data also suggest that other POLγA mutations affecting the interactions with POLγB or *vice versa* (e.g. mutations in POLγB affecting the interaction with POLγA) may be subjected to LONP1 degradation.

DISCUSSION

Mutations in *POLG* are a relatively common cause of a spectrum of mitochondrial disease. The substantial lack of relevant *in vivo* models has hampered our understanding of the pathogenesis of these *POLG*-related disorders. Here we developed a mouse model for human POLG^{A467T} and study the molecular pathogenesis of this common mutation *in vivo.* We complemented this analysis with detailed biochemical characterization of the corresponding events *in vitro*.

The mouse model revealed a clear effect on mtDNA replication in homozygous *Polg*$^{A449T/A449T}$ mice compared to WT controls. In mutant mouse tissues, we observed a reduction of 7S DNA and increased levels of RIs. Similar effects have previously been described in knock-out models for other components of the mitochondrial replication machinery, including POLγB (44); mtSSB (45); and TWINKLE (46). In addition, experiments carried out on *Polg*$^{A449T/A449T}$ MEFs revealed a striking reduction of mtDNA recovery after depletion with EtBr, thus demonstrating that POLγ activity is severely impaired in the mouse model, similar to what was described in human fibroblasts harboring distinct POLγ mutations (47). Surprisingly, despite these clear biochemical consequences, the mutant mouse model displayed very mild phenotypes compared to patients. We observed no reduction of lifespan or any obvious age-related phenotypes. In addition, the mutant mice were resilient to various challenges, including administration of valproate. The only obvious phenotype seen was after administration of CCl_4, which resulted in a slightly reduced recovery rate to liver damage, demonstrating that effective mtDNA replication is necessary for liver regeneration. Similar results have previously been reported for a knockout mouse model of mitochondrial topoisomerase I (TOP1mt) (48). Although we do not have an obvious explanation for the phenotypic differences between POLγ-defective mice and patients, our

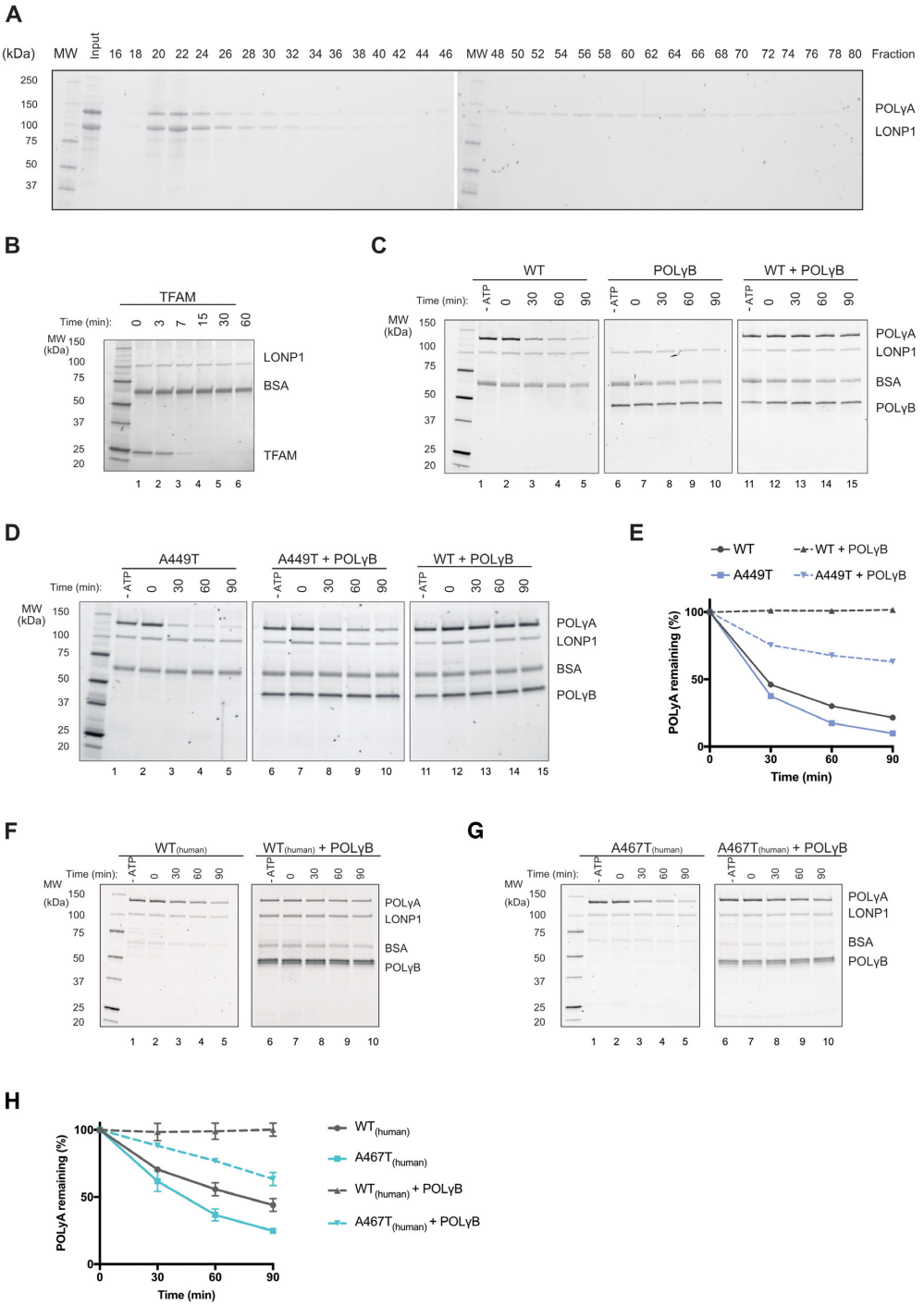

Figure 7. POLγA is a target of LONP1 degradation *in vitro*. (**A**) Size-exclusion chromatography of the complex formed by human LONP1^{S855A} (catalytic dead mutant) and hPOLγA^{WT}. The mixture was incubated for 10 min, at 37°C, in the presence of 10 mM $MgCl_2$ and 2 mM ATP before loaded on the chromatography. (**B**) SDS-PAGE of the LONP1 proteolysis assay of TFAM, over time. The reactions were incubated for the indicated times (top). (**C**) SDS-PAGE of the LONP1 proteolysis assay of isolated mPOLγA^{WT} (left), mPOLγB (middle), and mPOLγA^{WT} complexed with mPOLγB, over time. The reactions were incubated for the indicated times (top). In the absence of ATP (-ATP control), LONP1 does not exert proteolysis. (**D**) SDS-PAGE of the LONP1 proteolysis assay of mPOLγA^{A449T} in absence (left) or presence (middle) of mPOLγB, over time. Reactions with mPOLγA^{WT} + mPOLγB (right) were added for reference. The reactions were incubated for the indicated times (top). In the absence of ATP (-ATP control), LONP1 does not exert proteolysis. (**E**) Quantification of POLγA degradation over time (0–90 min) by LONP1, related to (C and D). mPOLγA^{WT} (black) and mPOLγA^{A449T} (blue), in absence (solid line) or presence (dashed line) of POLγB. Data are presented as mean ± SD. ($n = 3$). (**F**) SDS-PAGE of the LONP1 proteolysis assay of hPOLγA^{WT} in absence (left) or presence (right) of hPOLγB, over time. The reactions were incubated for the indicated times (top). In the absence of ATP (-ATP control), LONP1 does not exert proteolysis. (**G**) SDS-PAGE of the LONP1 proteolysis assay of hPOLγA^{A467T} in absence (left) or presence (right) of hPOLγB, over time. The reactions were incubated for the indicated times (top). In the absence of ATP (-ATP control), LONP1 does not exert proteolysis. (**H**) Quantification of human POLγA degradation over time (0–90 min) by LONP1, related to (F and G). hPOLγA^{WT} (gray) and hPOLγA^{A467T} (blue), in absence (solid line) or presence (dashed line) of POLγB. Data are presented as mean ± SD. (n = 3).

results suggest that the mutant mice may have effective compensatory mechanisms which mitigates POLγ dysfunction.

In agreement with the effect on mtDNA replication observed *in vivo,* our analysis of mPOLγA^{A449T} *in vitro* revealed a decrease in exonuclease and polymerase activities, which were partially rescued in the presence of POLγB. This observation highlights the importance of POLγB for the activity of POLγA. Interestingly, a comparison between the mouse POLγA^{A449T} and human POLγA^{A467T} proteins, revealed similar but more pronounced replication defects for the human polymerase, which can also help to explain why the human A467T mutation causes more severe phenotypes in affected patients (Figure 5H and I; Supplementary Figure S7C and D). These findings also demonstrate that the mouse model reproduces the molecular signature of the human disease, despite the milder phenotypes observed.

Interestingly, we noticed a reduction of POLγA^{A449T} protein levels in mouse tissues, and thus investigated the possible causes of this reduction. Using a thermofluor stability assay, we found that in isolation, POLγA is structurally unstable at physiological temperatures, but strongly stabilized in complex with POLγB. Size-exclusion chromatography demonstrates that the A449T mutation impairs interactions between POLγA and POLγB, disturbing POLγ holoenzyme formation. This latter observation is supported by structural modeling of A449T, which is situated in a region of POLγA required for interactions with POLγB. In our thermofluor analysis, we also noted a slight destabilization of POLγA^{A449T} at lower temperatures. Guided by these observations, we hypothesized that POLγA^{A449T} is a target for LONP1, a mitochondrial protease that degrades misfolded proteins.

The idea that POLγA^{A449T} is a substrate of LONP1 and that POLγB serves as a stabilizing, protective factor, were supported by both *in vitro* biochemical evidence and *in vivo* observations. Notably, depletion of LONP1 causes an increase in POLγA levels in both mouse tissues and human cells. In contrast, depletion of POLγB leads to lower levels of POLγA, whereas depletion of POLγA has no discernible effect on POLγB. In this context, it should be noted that we cannot rule out that other proteases can contribute to POLγA degradation *in vivo* (49).

In addition, the superstoichiometric levels of POLγB relative to POLγA in human cells and mouse tissues, also supports the idea that POLγB protects POLγA from proteolysis. The rapid degradation of POLγA in the absence of POLγB could be of physiological relevance, since on its own, the POLγA displays low polymerase activity but high exonuclease activity, which may disturb mtDNA replication.

In our experiments, we noted that depletion of either POLγA or POLγB resulted in increased levels of LONP1. The exact cause of this effect is unclear, but LONP1 has many other targets *in vivo* and is required for multiple mitochondrial functions. We therefore hypothesize that the increase is a part of a more general stress response, similar to what has been suggested previously (50).

Furthermore, during analysis, we also noted that native POLγB run at a slightly higher molecular weight than expected. The reason for the difference between the predicted and observed size of the protein is not known to us, but could indicate that the cleavage site for the leader peptide is different from what has previously been predicted in the literature. Alternatively, POLγB may contain post-translational modifications that affect its migration in SDS-PAGE. Clarifying this point warrants additional work and may have consequences for our understanding of POLγ function.

In conclusion, we here describe in detail the *in vivo* and *in vitro* features of a common POLγA mutation, with potential implications for the pathogenesis of a previously poorly understood condition. Our findings imply that mutations in *POLG1* or *POLG2* that cause weaker interactions within the POLγ holoenzyme will lead to degradation of POLγA, resulting in protein depletion *in vivo*. We speculate that interventions aimed at increasing POLγA stability, either by directly stabilizing the protein or increasing interactions with POLγB may have therapeutic value in affected patients.

DATA AVAILABILITY

The data that support the findings of this work are available from the corresponding authors upon request.

SUPPLEMENTARY DATA

Supplementary Data are available at NAR Online.

ACKNOWLEDGEMENTS

The authors would like to thank Jay P Uhler for generating the graphical abstract.

FUNDING

Telethon Foundation [GGP19007 to M.Z. and 20013 to CV]; Fondation NRJ pour les Neurosciences - Institute de France Grant (to M.Z.); Associazione Luigi Comini Onlus (to M.Z., C.V.); Medical Research Council (MRC) [MC_UU_00015/5, MC_UU_00015/4, MC_UU_00015/7]; Marie Sklodowska-Curie ITN-REMIX [721757 to P.S.P., C.P.H., D.H.H.]; Swedish Research Council [2018-02439 to M.F.]; Swedish Cancer Foundation [2019-816 to M.F.]; European Research Council [2016-683191 to M.F].; Knut and Alice Wallenberg Foundation [KAW 2017.0080 to M.F.]; MRC Graduate Student Fellowship (to L.T.); EMBO Installation Grant [IG4149, TUBITAK 119C022 to Sukru Anil Dogan (SAD)]; Bogazici University [SUP-15501 to S.A.D.]. Funding for open access charge: Telethon Foundation; ERC.
Conflict of interest statement. None declared.

REFERENCES

1. Gustafsson,C.M., Falkenberg,M. and Larsson,N.G. (2016) Maintenance and expression of mammalian mitochondrial DNA. *Annu. Rev. Biochem.*, **85**, 133–160.
2. Longley,M.J., Prasad,R., Srivastava,D.K., Wilson,S.H. and Copeland,W.C. (1998) Identification of 5'-deoxyribose phosphate lyase activity in human DNA polymerase gamma and its role in mitochondrial base excision repair in vitro. *Proc. Natl Acad. Sci. U.S.A.*, **95**, 12244–12248.

3. Ropp,P.A. and Copeland,W.C. (1996) Cloning and characterization of the human mitochondrial DNA polymerase, DNA polymerase gamma. *Genomics*, **36**, 449–458.
4. Lim,S.E., Longley,M.J. and Copeland,W.C. (1999) The mitochondrial p55 accessory subunit of human DNA polymerase gamma enhances DNA binding, promotes processive DNA synthesis, and confers N-ethylmaleimide resistance. *J. Biol. Chem.*, **274**, 38197–38203.
5. Spelbrink,J.N., Li,F.Y., Tiranti,V., Nikali,K., Yuan,Q.P., Tariq,M., Wanrooij,S., Garrido,N., Comi,G., Morandi,L. *et al.* (2001) Human mitochondrial DNA deletions associated with mutations in the gene encoding Twinkle, a phage T7 gene 4-like protein localized in mitochondria. *Nat. Genet.*, **28**, 223–231.
6. Korhonen,J.A., Gaspari,M. and Falkenberg,M. (2003) TWINKLE Has 5' → 3' DNA helicase activity and is specifically stimulated by mitochondrial single-stranded DNA-binding protein. *J. Biol. Chem.*, **278**, 48627–48632.
7. Ferrari,G., Lamantea,E., Donati,A., Filosto,M., Briem,E., Carrara,F., Parini,R., Simonati,A., Santer,R. and Zeviani,M. (2005) Infantile hepatocerebral syndromes associated with mutations in the mitochondrial DNA polymerase-gammaA. *Brain*, **128**, 723–731.
8. de Vries,M.C., Rodenburg,R.J., Morava,E., van Kaauwen,E.P., ter Laak,H., Mullaart,R.A., Snoeck,I.N., van Hasselt,P.M., Harding,P., van den Heuvel,L.P. *et al.* (2007) Multiple oxidative phosphorylation deficiencies in severe childhood multi-system disorders due to polymerase gamma (POLG1) mutations. *Eur. J. Pediatr.*, **166**, 229–234.
9. Horvath,R., Hudson,G., Ferrari,G., Futterer,N., Ahola,S., Lamantea,E., Prokisch,H., Lochmuller,H., McFarland,R., Ramesh,V. *et al.* (2006) Phenotypic spectrum associated with mutations of the mitochondrial polymerase gamma gene. *Brain*, **129**, 1674–1684.
10. Nguyen,K.V., Sharief,F.S., Chan,S.S., Copeland,W.C. and Naviaux,R.K. (2006) Molecular diagnosis of Alpers syndrome. *J. Hepatol.*, **45**, 108–116.
11. Chan,S.S., Longley,M.J. and Copeland,W.C. (2005) The common A467T mutation in the human mitochondrial DNA polymerase (POLG) compromises catalytic efficiency and interaction with the accessory subunit. *J. Biol. Chem.*, **280**, 31341–31346.
12. Uusimaa,J., Gowda,V., McShane,A., Smith,C., Evans,J., Shrier,A., Narasimhan,M., O'Rourke,A., Rajabally,Y., Hedderly,T. *et al.* (2013) Prospective study of POLG mutations presenting in children with intractable epilepsy: prevalence and clinical features. *Epilepsia*, **54**, 1002–1011.
13. Viscomi,C. and Zeviani,M. (2017) MtDNA-maintenance defects: syndromes and genes. *J. Inherit. Metab. Dis.*, **40**, 587–599.
14. Rahman,S. and Copeland,W.C. (2019) POLG-related disorders and their neurological manifestations. *Nat. Rev. Neurol.*, **15**, 40–52.
15. DeBalsi,K.L., Longley,M.J., Hoff,K.E. and Copeland,W.C. (2017) Synergistic effects of the in cis T251I and P587L mitochondrial DNA polymerase gamma disease mutations. *J. Biol. Chem.*, **292**, 4198–4209.
16. Rajakulendran,S., Pitceathly,R.D., Taanman,J.W., Costello,H., Sweeney,M.G., Woodward,C.E., Jaunmuktane,Z., Holton,J.L., Jacques,T.S., Harding,B.N. *et al.* (2016) A clinical, neuropathological and genetic study of homozygous A467T POLG-related mitochondrial disease. *PLoS One*, **11**, e0145500.
17. Tzoulis,C., Engelsen,B.A., Telstad,W., Aasly,J., Zeviani,M., Winterthun,S., Ferrari,G., Aarseth,J.H. and Bindoff,L.A. (2006) The spectrum of clinical disease caused by the A467T and W748S POLG mutations: a study of 26 cases. *Brain*, **129**, 1685–1692.
18. Pinti,M., Gibellini,L., Nasi,M., De Biasi,S., Bortolotti,C.A., Iannone,A. and Cossarizza,A. (2016) Emerging role of Lon protease as a master regulator of mitochondrial functions. *Biochim. Biophys. Acta*, **1857**, 1300–1306.
19. Larsson,N.G., Wang,J., Wilhelmsson,H., Oldfors,A., Rustin,P., Lewandoski,M., Barsh,G.S. and Clayton,D.A. (1998) Mitochondrial transcription factor A is necessary for mtDNA maintenance and embryogenesis in mice. *Nat. Genet.*, **18**, 231–236.
20. Farge,G., Mehmedovic,M., Baclayon,M., van den Wildenberg,S.M., Roos,W.H., Gustafsson,C.M., Wuite,G.J. and Falkenberg,M. (2014) In vitro-reconstituted nucleoids can block mitochondrial DNA replication and transcription. *Cell Rep.*, **8**, 66–74.
21. Lu,B., Lee,J., Nie,X., Li,M., Morozov,Y.I., Venkatesh,S., Bogenhagen,D.F., Temiakov,D. and Suzuki,C.K. (2013) Phosphorylation of human TFAM in mitochondria impairs DNA binding and promotes degradation by the AAA+ Lon protease. *Mol. Cell*, **49**, 121–132.
22. Alam,T.I., Kanki,T., Muta,T., Ukaji,K., Abe,Y., Nakayama,H., Takio,K., Hamasaki,N. and Kang,D. (2003) Human mitochondrial DNA is packaged with TFAM. *Nucleic Acids Res.*, **31**, 1640–1645.
23. Peter,B., Waddington,C.L., Olahova,M., Sommerville,E.W., Hopton,S., Pyle,A., Champion,M., Ohlson,M., Siibak,T., Chrzanowska-Lightowlers,Z.M.A. *et al.* (2018) Defective mitochondrial protease LonP1 can cause classical mitochondrial disease. *Hum. Mol. Genet.*, **27**, 1743–1753.
24. Nagashima,S., Tabara,L.C., Tilokani,L., Paupe,V., Anand,H., Pogson,J.H., Zunino,R., McBride,H.M. and Prudent,J. (2020) Golgi-derived PI(4)P-containing vesicles drive late steps of mitochondrial division. *Science*, **367**, 1366–1371.
25. Bugiani,M., Invernizzi,F., Alberio,S., Briem,E., Lamantea,E., Carrara,F., Moroni,I., Farina,L., Spada,M., Donati,M.A. *et al.* (2004) Clinical and molecular findings in children with complex I deficiency. *Biochim. Biophys. Acta*, **1659**, 136–147.
26. Fernandez-Vizarra,E., Lopez-Perez,M.J. and Enriquez,J.A. (2002) Isolation of biogenetically competent mitochondria from mammalian tissues and cultured cells. *Methods*, **26**, 292–297.
27. Calvaruso,M.A., Smeitink,J. and Nijtmans,L. (2008) Electrophoresis techniques to investigate defects in oxidative phosphorylation. *Methods*, **46**, 281–287.
28. Sciacco,M. and Bonilla,E. (1996) Cytochemistry and immunocytochemistry of mitochondria in tissue sections. *Methods Enzymol.*, **264**, 509–521.
29. Reyes,A., Kazak,L., Wood,S.R., Yasukawa,T., Jacobs,H.T. and Holt,I.J. (2013) Mitochondrial DNA replication proceeds via a 'bootlace' mechanism involving the incorporation of processed transcripts. *Nucleic Acids Res.*, **41**, 5837–5850.
30. Farge,G., Pham,X.H., Holmlund,T., Khorostov,I. and Falkenberg,M. (2007) The accessory subunit B of DNA polymerase gamma is required for mitochondrial replisome function. *Nucleic Acids Res.*, **35**, 902–911.
31. Al-Behadili,A., Uhler,J.P., Berglund,A.K., Peter,B., Doimo,M., Reyes,A., Wanrooij,S., Zeviani,M. and Falkenberg,M. (2018) A two-nuclease pathway involving RNase H1 is required for primer removal at human mitochondrial OriL. *Nucleic Acids Res.*, **46**, 9471–9483.
32. Matulis,D., Kranz,J.K., Salemme,F.R. and Todd,M.J. (2005) Thermodynamic stability of carbonic anhydrase: measurements of binding affinity and stoichiometry using ThermoFluor. *Biochemistry*, **44**, 5258–5266.
33. Saneto,R.P., Lee,I.C., Koenig,M.K., Bao,X., Weng,S.W., Naviaux,R.K. and Wong,L.J. (2010) POLG DNA testing as an emerging standard of care before instituting valproic acid therapy for pediatric seizure disorders. *Seizure*, **19**, 140–146.
34. Stewart,J.D., Horvath,R., Baruffini,E., Ferrero,I., Bulst,S., Watkins,P.B., Fontana,R.J., Day,C.P. and Chinnery,P.F. (2010) Polymerase gamma gene POLG determines the risk of sodium valproate-induced liver toxicity. *Hepatology*, **52**, 1791–1796.
35. Bogenhagen,D. and Clayton,D.A. (1978) Mechanism of mitochondrial DNA replication in mouse L-cells: kinetics of synthesis and turnover of the initiation sequence. *J. Mol. Biol.*, **119**, 49–68.
36. Doda,J.N., Wright,C.T. and Clayton,D.A. (1981) Elongation of displacement-loop strands in human and mouse mitochondrial DNA is arrested near specific template sequences. *Proc. Natl Acad. Sci. U.S.A.*, **78**, 6116–6120.
37. Nicholls,T.J. and Minczuk,M. (2014) In D-loop: 40 years of mitochondrial 7S DNA. *Exp. Gerontol.*, **56**, 175–181.
38. Do,Y., Matsuda,S., Inatomi,T., Nakada,K., Yasukawa,T. and Kang,D. (2020) The accessory subunit of human DNA polymerase gamma is required for mitochondrial DNA maintenance and is able to stabilize the catalytic subunit. *Mitochondrion*, **53**, 133–139.
39. Lee,Y.S., Kennedy,W.D. and Yin,Y.W. (2009) Structural insight into processive human mitochondrial DNA synthesis and disease-related polymerase mutations. *Cell*, **139**, 312–324.
40. Bezawork-Geleta,A., Brodie,E.J., Dougan,D.A. and Truscott,K.N. (2015) LON is the master protease that protects against protein aggregation in human mitochondria through direct degradation of misfolded proteins. *Sci. Rep.*, **5**, 17397–17410.
41. Kereiche,S., Kovacik,L., Bednar,J., Pevala,V., Kunova,N., Ondrovicova,G., Bauer,J., Ambro,L., Bellova,J., Kutejova,E. *et al.*

(2016) The N-terminal domain plays a crucial role in the structure of a full-length human mitochondrial Lon protease. *Sci. Rep.*, **6**, 33631–33640.
42. Matsushima,Y., Goto,Y. and Kaguni,L.S. (2010) Mitochondrial Lon protease regulates mitochondrial DNA copy number and transcription by selective degradation of mitochondrial transcription factor A (TFAM). *Proc. Natl Acad. Sci. U.S.A.*, **107**, 18410–18415.
43. Macao,B., Uhler,J.P., Siibak,T., Zhu,X., Shi,Y., Sheng,W., Olsson,M., Stewart,J.B., Gustafsson,C.M. and Falkenberg,M. (2015) The exonuclease activity of DNA polymerase gamma is required for ligation during mitochondrial DNA replication. *Nat. Commun.*, **6**, 73037312.
44. Di Re,M., Sembongi,H., He,J., Reyes,A., Yasukawa,T., Martinsson,P., Bailey,L.J., Goffart,S., Boyd-Kirkup,J.D., Wong,T.S. *et al.* (2009) The accessory subunit of mitochondrial DNA polymerase gamma determines the DNA content of mitochondrial nucleoids in human cultured cells. *Nucleic Acids Res.*, **37**, 5701–5713.
45. Ruhanen,H., Borrie,S., Szabadkai,G., Tyynismaa,H., Jones,A.W., Kang,D., Taanman,J.W. and Yasukawa,T. (2010) Mitochondrial single-stranded DNA binding protein is required for maintenance of mitochondrial DNA and 7S DNA but is not required for mitochondrial nucleoid organisation. *Biochim. Biophys. Acta*, **1803**, 931–939.
46. Milenkovic,D., Matic,S., Kuhl,I., Ruzzenente,B., Freyer,C., Jemt,E., Park,C.B., Falkenberg,M. and Larsson,N.G. (2013) TWINKLE is an essential mitochondrial helicase required for synthesis of nascent D-loop strands and complete mtDNA replication. *Hum. Mol. Genet.*, **22**, 1983–1993.
47. Stewart,J.D., Schoeler,S., Sitarz,K.S., Horvath,R., Hallmann,K., Pyle,A., Yu-Wai-Man,P., Taylor,R.W., Samuels,D.C., Kunz,W.S. *et al.* (2011) POLG mutations cause decreased mitochondrial DNA repopulation rates following induced depletion in human fibroblasts. *Biochim. Biophys. Acta*, **1812**, 321–325.
48. Khiati,S., Baechler,S.A., Factor,V.M., Zhang,H., Huang,S.Y., Dalla Rosa,I., Sourbier,C., Neckers,L., Thorgeirsson,S.S. and Pommier,Y. (2015) Lack of mitochondrial topoisomerase I (TOP1mt) impairs liver regeneration. *Proc. Natl Acad. Sci. U.S.A.*, **112**, 11282–11287.
49. Lee,Y.G., Kim,H.W., Nam,Y., Shin,K.J., Lee,Y.J., Park,D.H., Rhee,H.W., Seo,J.K. and Chae,Y.C. (2021) LONP1 and ClpP cooperatively regulate mitochondrial proteostasis for cancer cell survival. *Oncogenesis*, **10**, 18–31.
50. Zurita Rendon,O. and Shoubridge,E.A. (2018) LONP1 Is Required for Maturation of a Subset of Mitochondrial Proteins, and Its Loss Elicits an Integrated Stress Response. *Mol. Cell. Biol.*, **38**, e00412-17.